Available online at www.sciencedirect.com
SCIENCE DIRECT®
Journal of Sound and Vibration 282 (2005) 1–35
JOURNAL OF SOUND AND VIBRATION
www.elsevier.com/locate/jsvi

Parametric estimation of the cross-power spectral density

Kenji Kanazawa*, Kazuta Hirata

Civil Engineering Research Laboratory, Central Research Institute of Electric Power Industry, 1646 Abiko, Abiko-shi, Chiba-ken 270-1194, Japan

Received 14 August 2002; received in revised form 10 February 2004; accepted 13 February 2004
Available online 15 September 2004

Abstract

A new cross-spectral analysis procedure is proposed for the parametric estimation of the relationship between two time sequences in the frequency domain. In this method, the two observable outputs are modeled as a pair of autoregressive moving-average and moving-average (ARMAMA) models under the assumption that the two outputs are driven by a common input and independent ones simultaneously. Cross- and auto-power spectral densities (PSDs) of a pair of ARMAMA models can be derived as forms of rational polynomial functions. The coefficients of these functions can be estimated from the cross-correlation function or the auto-correlation functions of the two observed sequences by using the method presented in this paper. The main advantage of the present procedure is that the physical parameters of an unknown system can be easily estimated from the coefficients of the cross- and auto-PSD functions. To illustrate the effectiveness of the proposed procedure, numerical and practical examples of a mechanical vibration problem are analyzed. The results show that the proposed procedure gives accurate cross- and auto-PSD estimates. Moreover, the physical properties of the unknown system can be well estimated from the obtained cross- and auto-PSDs.

1. Introduction

Cross-spectral analysis is a fundamental and powerful procedure to investigate an unknown relationship between two time series in the frequency domain. It is especially effective for the

*Corresponding author. Tel.: +81-4-7182-1181; fax: +81-4-7184-2941.
E-mail address: kanazawa@criepi.denken.or.jp (K. Kanazawa).

0022-460X/$ - see front matter © 2004 Elsevier Ltd. All rights reserved.
doi:10.1016/j.jsv.2004.02.009

estimation of correlated periodic components between two measured records contaminated by uncorrelated noises. Thus, to take advantage of the feature, the cross spectrum is widely employed in many engineering problems; e.g., for the analysis of feedback systems [1], atmospheric problems [2], time delay estimation of spatial sensors [3], blind equalization in communications [4], and system identification of mechanical vibration systems [5]. In such multivariate problems when the input cannot be specified, the authors believe cross-spectral analysis is more effective than auto-spectral analysis or transfer function-based analysis, because the unknown relationship of sequences can be evaluated without a priori definition of input and output, which is required in transfer-based analysis. Whereas in Refs. [1–5] the cross-spectral density is computed in a non-parametric way, by using the Fast Fourier Transform FFT, in this paper, a parametric approach will be developed for cross-spectral analysis.

For estimating the auto-power spectral density (auto-PSD) in the parametric approach, various schemes have been proposed based on scalar linear differential models such as autoregressive (AR) models or autoregressive moving-average (ARMA) models [6–14]. Additionally, for estimating the transfer function between two sequences, there are various schemes based on AR models with the extra input (ARX) or autoregressive moving-average models with the extra input (ARMAX) [15,16]. Using these parametric schemes, one can estimate the auto-PSD or transfer function with coefficients of rational polynomial functions. From these coefficients, the physical parameters can often be identified directly. Therefore, in such types of engineering problems, these parametric schemes are useful for system identification; e.g., in mechanical vibration problems, by using the linear differential model, the eigenvalues and eigenvectors of a system can be estimated from the vibration response data [17].

While there are considerable studies on auto-PSD or transfer function estimates, very little attention has been paid to the parametric approach to cross-PSD estimates. In practice, the cross-PSD is often computed by a non-parametric procedure such as the FFT [18,19]. For a multivariate system, conventional schemes of a scalar linear differential model have been extended to vector-based schemes [20–23]. However, these vector-based schemes are complicated in such extensions, because unknown parameters must be treated as matrix representation. Moreover, it is generally difficult to explain physical meanings of the unknown system from the obtained parameter matrices, even if the vector linear differential equations are well estimated. On the other hand, the scalar scheme can be handled rather easily, and the multivariate system can be analyzed in the repetitive use of the scalar scheme.

We propose a parametric approach for the analysis of the cross- and auto-PSDs, using a pair of linear differential models for the two output sequences. The models are composed of MA terms added to an ARMA model, therefore, they are called the autoregressive moving-average and moving-average (ARMAMA) model. Specifically, throughout the paper, the cross- and auto-PSDs will be treated as two-sided spectral density functions $S_{xy}(\omega)$ and $S_{xx}(\omega)$ defined by [24]

$$S_{xy}(\omega) = \int_{-\infty}^{\infty} R_{xy}(\tau)\mathrm{e}^{-\mathrm{j}\omega\tau}\,\mathrm{d}\tau \quad \text{and} \quad S_{xx}(\omega) = \int_{-\infty}^{\infty} R_{xx}(\tau)\mathrm{e}^{-\mathrm{j}\omega\tau}\,\mathrm{d}\tau, \tag{1}$$

where ω is the circular frequency; $\mathrm{j} = \sqrt{-1}$; $R_{xy}(\tau)$ and $R_{xx}(\tau)$ are the covariance functions associated with stationary random variables $x(t)$ and $y(t)$. The covariance functions of $x(t)$ and

$y(t)$ will be also defined by

$$R_{xy}(\tau) = E[x(t)y(t+\tau)] \quad \text{and} \quad R_{xx}(\tau) = E[x(t)x(t+\tau)], \tag{2}$$

where $E[\cdot]$ denotes the expectation operator on t.

The outline of the paper is as follows. In Section 2, the definition of the ARMAMA model and its differential form are presented. In Section 3, the representation of the cross-PSD between the two ARMAMA models is developed and also a procedure for estimation of the cross-PSD. In Section 4, the authors derive the representation and a procedure for estimation of the auto-PSD within the use of the correlated terms given by the computation of the cross-PSD in Section 3. In Section 5, the authors discuss the structural difference between the ARMAMA model and multivariate linear difference models. Section 6 presents some numerical examples to illustrate the application of the proposed procedure. Furthermore, the practicality of the procedure will be discussed in Section 7 and Section 8 concludes the paper.

2. Definition of ARMAMA model

Let $x(t)$ and $y(t)$ be observable output sequences of two stationary processes. The ARMAMA models are defined in discrete time t as

$$x(t) = \frac{B_x(z^{-1})}{A_x(z^{-1})}\, e(t) + \frac{D_x(z^{-1})}{C_x(z^{-1})}\, e_x(t) \tag{3}$$

$$= \frac{\sum_{j=0}^{m_b} b_x(j) z^{-j}}{\sum_{j=0}^{m_a} a_x(j) z^{-j}}\, e(t) + \frac{\sum_{j=0}^{m_d} d_x(j) z^{-j}}{\sum_{j=0}^{m_c} c_x(j) z^{-j}}\, e_x(t), \tag{4}$$

$$y(t) = \frac{B_y(z^{-1})}{A_y(z^{-1})}\, e(t) + \frac{D_y(z^{-1})}{C_y(z^{-1})}\, e_y(t) \tag{5}$$

$$= \frac{\sum_{j=0}^{n_b} b_y(j) z^{-j}}{\sum_{j=0}^{n_a} a_y(j) z^{-j}}\, e(t) + \frac{\sum_{j=0}^{n_d} d_y(j) z^{-j}}{\sum_{j=0}^{n_c} c_y(j) z^{-j}}\, e_y(t), \tag{6}$$

$$a_x(0) = 1, \quad a_y(0) = 1, \quad c_x(0) = 1, \quad c_y(0) = 1, \tag{7}$$

where $e(t)$, $e_x(t)$ and $e_y(t)$ are the unobservable inputs of white noise sequences with zero mean and unit variance, which are mutually independent; z is the unit-delay operator; $a_x(j)$, $a_y(j)$, $c_x(j)$ and $c_y(j)$ are the AR coefficients; $b_x(j)$, $b_y(j)$, $d_x(j)$ and $d_y(j)$ are the MA coefficients. Fig. 1 shows a block diagram of the ARMAMA models.

In Eqs. (3) and (5), both outputs $x(t)$ and $y(t)$ are driven by the common input $e(t)$ given as the first term of the right-hand sides in each equation; i.e., these terms can represent correlated components between $x(t)$ and $y(t)$. Additionally, each output is also driven by different inputs $e_x(t)$ or $e_y(t)$ given as the second terms of Eqs. (4) or (6), which can represent uncorrelated components between two outputs. As described in the next section, in the analysis of cross-PSD the first term in Eqs. (4) and (6) plays an important role, and the second term vanishes due to the assumption of mutual independence between $e(t)$, $e_x(t)$ and $e_y(t)$. On the other hand, in the analysis of auto-PSD both the first and the second terms in Eqs. (4) and (6) are required.

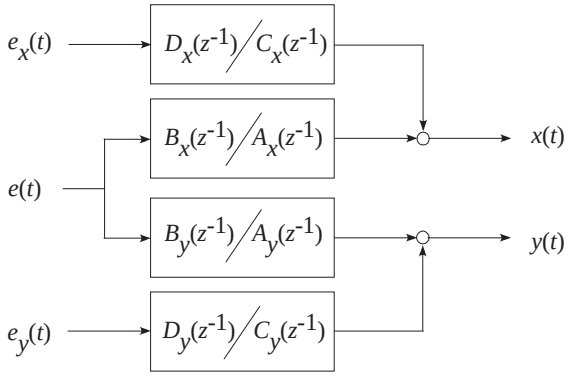

Fig. 1. Block diagram of the ARMAMA model.

Eqs. (4) and (6) can be rewritten in the linear difference forms as

$$\sum_{j=0}^{m_c}\sum_{k=0}^{m_a} c_x(j)a_x(k)x(t-j-k) = \sum_{j=0}^{m_c}\sum_{k=0}^{m_b} c_x(j)b_x(k)e(t-j-k) + \sum_{j=0}^{m_d}\sum_{k=0}^{m_a} d_x(j)a_x(k)e_x(t-j-k), \tag{8}$$

$$\sum_{j=0}^{n_c}\sum_{k=0}^{n_a} c_y(j)a_y(k)y(t-j-k) = \sum_{j=0}^{n_c}\sum_{k=0}^{n_b} c_y(j)b_y(k)e(t-j-k) + \sum_{j=0}^{n_d}\sum_{k=0}^{n_a} d_y(j)a_y(k)e_y(t-j-k). \tag{9}$$

Each model in Eqs. (8) and (9) consists of one AR term and two MA terms; therefore, the authors propose to call them ARMAMA models.

3. Computation of cross-PSD based on ARMAMA model

This section develops the procedure for the cross-PSD estimation of the ARMAMA model. Firstly, using the impulse response equivalent to the ARMAMA model, the general representation of the cross-PSD will be derived. In the representation, the cross-PSD is expressed as a rational function of the AR and the MA coefficients. However, it is difficult to estimate the MA coefficients by using only the observed outputs. This is because both the time sequence and its coefficients in the MA terms are unknown, and one must solve highly nonlinear functions to estimate these unknown parameters [22,25]. Some iterative schemes have been proposed for solving the highly nonlinear functions of the ARMA model; e.g., the bootstrap method or the maximum likelihood estimation [16,25], but these schemes cannot be easily handled in practice. Thus, to take an easier approach, we will rewrite the simple representation of the cross-PSD

without the use of the MA coefficients; i.e., the cross-PSD is rewritten as a function of the AR coefficients and the cross-correlation function of the observed outputs. Finally, a set of equations for the AR coefficients will be shown.

3.1. Derivation of general cross-PSD form

Eqs. (3) and (5) can be alternatively expressed by using the impulse response functions below:

$$x(t) = H_{bx}(z^{-1})e(t) + H_{dx}(z^{-1})e_x(t), \tag{10}$$

$$y(t) = H_{by}(z^{-1})e(t) + H_{dy}(z^{-1})e_y(t), \tag{11}$$

where

$$H_{bx}(z^{-1}) = \sum_{j=0}^{\infty} h_{bx}(j)z^{-j} \equiv \frac{B_x(z^{-1})}{A_x(z^{-1})}, \tag{12}$$

$$H_{by}(z^{-1}) = \sum_{j=0}^{\infty} h_{by}(j)z^{-j} \equiv \frac{B_y(z^{-1})}{A_x(z^{-1})}, \tag{13}$$

$$H_{dx}(z^{-1}) = \sum_{j=0}^{\infty} h_{dx}(j)z^{-j} \equiv \frac{D_x(z^{-1})}{C_x(z^{-1})}, \tag{14}$$

$$H_{dy}(z^{-1}) = \sum_{j=0}^{\infty} h_{dy}(j)z^{-j} \equiv \frac{D_y(z^{-1})}{C_y(z^{-1})} \tag{15}$$

and $\{h_{bx}(j)\}$, $\{h_{by}(j)\}$, $\{h_{dx}(j)\}$ and $\{h_{dy}(j)\}$ are the impulse response sequences of the transfer functions $B_x(z^{-1})/A_x(z^{-1})$, $B_y(z^{-1})/A_y(z^{-1})$, $D_x(z^{-1})/C_x(z^{-1})$ and $D_y(z^{-1})/C_y(z^{-1})$, respectively. Eqs. (10) and (11) can be rewritten in difference form as

$$x(t) = \sum_{j=0}^{\infty} h_{bx}(j)e(t-j) + \sum_{j=0}^{\infty} h_{dx}(j)e_x(t-j), \tag{16}$$

$$y(t) = \sum_{k=0}^{\infty} h_{by}(k)e(t-k) + \sum_{k=0}^{\infty} h_{dy}(k)e_y(t-k). \tag{17}$$

The cross-correlation function $R_{xy}(\tau)$ of $x(t)$ and $y(t)$ is given from Eqs. (16) and (17) as

$$\begin{aligned} R_{xy}(\tau) &= E[x(t)\,y(t+\tau)] \\ &= \sum_{j=0}^{\infty}\sum_{k=0}^{\infty} h_{bx}(j)h_{by}(k)E[e(t-j)\,e(t+\tau-k)] \\ &= \sum_{j=0}^{\infty} h_{bx}(j)h_{by}(j+\tau). \end{aligned} \tag{18}$$

In the derivation of the equation above, the assumption that $e(t)$, $e_x(t)$ and $e_y(t)$ are mutually independent is used.

Then, the corresponding cross-PSD $S_{xy}(z^{-1})$ between $x(t)$ and $y(t)$ is given by the Wiener–Khinchin theorem as

$$S_{xy}(z^{-1}) = \sum_{\tau=-\infty}^{\infty} R_{xy}(\tau) z^{-\tau}. \tag{19}$$

Since the impulse responses $h_{bx}(t)$ and $h_{by}(t)$ are equal to zero for $t<0$, substitution of Eq. (18) into Eq. (19) leads to the equation below:

$$S_{xy}(z^{-1}) = \sum_{j=0}^{\infty} \sum_{\tau=-j}^{\infty} h_{bx}(j) h_{by}(j+\tau) z^{-\tau}. \tag{20}$$

Let $k = j + \tau$ and substitute Eqs. (12) and (13) into Eq. (20), then the cross-PSD between $x(t)$ and $y(t)$ can be obtained as follows:

$$\begin{aligned} S_{xy}(z^{-1}) &= \sum_{j=0}^{\infty} \sum_{k=0}^{\infty} h_{bx}(j) h_{by}(k) z^{-(k-j)} \\ &= H_{bx}(z) H_{by}(z^{-1}) \\ &= \frac{B_x(z) B_y(z^{-1})}{A_x(z) A_y(z^{-1})}. \end{aligned} \tag{21}$$

3.2. Simple representation of cross-PSD without MA coefficient

To estimate the cross-PSD from Eq. (21), the AR and MA coefficients $a_x(j)$, $a_y(j)$, $b_x(j)$ and $b_y(j)$ are required to be determined. In the case of ARMA model, Kinkel et al. [6], Kaveh [7], Kay [9] have proposed the procedure of auto-PSD estimation without determining of the MA coefficients. In a similar way, the cross-PSD in Eq. (21) can be modified into an alternative form without using MA coefficients.

The numerator in Eq. (21) can be expressed as

$$\begin{aligned} B_x(z) B_y(z^{-1}) &= \sum_{k=0}^{m_b} b_x(k) z^k \sum_{j=0}^{n_b} b_y(j) z^{-j} \\ &= \sum_{l=-m_b}^{n_b} \sum_{k=0}^{m_b} b_x(k) b_y(k+l) z^{-l}. \end{aligned} \tag{22}$$

Note that $j = k + l$; $b_y(j) = 0$ for $j<0$ or for $n_b<j$.

To simplify the derivation below, Eqs. (8) and (9) are rewritten by using two sets of new instrumental variables $u(t)$, $v(t)$ and $r(t)$, $s(t)$:

$$\sum_{k=0}^{m_a} a_x(k)(x(t-k) - u(t-k)) = \sum_{k=0}^{m_b} b_x(k) e(t-k) \equiv r(t), \tag{23}$$

$$\sum_{k=0}^{n_a} a_y(k)(y(t-k)-v(t-k)) = \sum_{k=0}^{n_b} b_y(k)e(t-k) \equiv s(t) \tag{24}$$

and

$$\sum_{j=0}^{m_c} c_x(j)u(t-j) = \sum_{j=0}^{m_d} d_x(j)e_x(t-j), \tag{25}$$

$$\sum_{j=0}^{n_c} c_y(j)v(t-j) = \sum_{j=0}^{n_d} d_y(j)e_y(t-j). \tag{26}$$

From the left-hand side of Eqs. (23) and (24), the cross-correlation function $R_{rs}(l)$ of $r(t)$ and $s(t)$ can be expressed as

$$\begin{aligned} R_{rs}(l) &= E[r(t)\cdot s(t+l)] \\ &= \sum_{k=0}^{m_a}\sum_{j=0}^{n_a} a_x(k)a_y(j)E[(x(t-k)-u(t-k))(y(t+l-j)-v(t+l-j))] \\ &= \sum_{k=0}^{m_a}\sum_{j=0}^{n_a} a_x(k)a_y(j)R_{xy}(l+k-j), \end{aligned} \tag{27}$$

where $R_{xy}(\tau)$ is the cross-correlation function of $x(t)$ and $y(t)$, which can be estimated from the time-series observation.[1] Note that the cross-correlation functions $R_{xv}(\tau)$ of $x(t)$ and $v(t)$, $R_{yu}(\tau)$ of $y(t)$ and $u(t)$ and $R_{uv}(\tau)$ of $u(t)$ and $v(t)$ equal to zero in all τ. (See Eqs. (A.3)–(A.5) in Appendix A.)

Next, from the right-hand side of Eqs. (23) and (24), the cross-correlation function $R_{rs}(l)$ can also be also expressed as

$$\begin{aligned} R_{rs}(l) &= E[r(t)\,s(t+l)] \\ &= \sum_{k=0}^{m_b}\sum_{j=0}^{n_b} b_x(k)b_y(j)E[e(t-k)\,e(t+l-j)] \\ &= \sum_{k=0}^{m_b} b_x(k)b_y(k+l). \end{aligned} \tag{28}$$

Then substituting Eq. (28) into Eq. (22), the alternative representation of cross-PSD in Eq. (21) can be obtained:

$$S_{xy}(z^{-1}) = \frac{\sum_{l=-m_b}^{n_b} R_{rs}(l)z^{-l}}{A_x(z)A_y(z^{-1})}. \tag{29}$$

Since $R_{rs}(l)$ can be computed for $l=-m_b,\ldots,n_b$ by using Eq. (27), the cross-PSD given by Eq. (29) can be evaluated without using MA coefficients.

[1] In the examples of Sections 5 and 6, the cross-correlation function of $x(t)$ and $y(t)$ is estimated below:

$$R_{xy}(\tau) = \frac{1}{N-1}\sum_{l=1}^{N-1} x(l)\,y(l+\tau).$$

3.3. Computation of AR coefficient

Multiplying both sides of Eq. (23) by $y(t-l)$ and taking expectation on t, we can obtain the equation below:

$$\sum_{k=0}^{m_a} a_x(k)R_{xy}(k-l) = \sum_{k=0}^{m_b} b_x(k)h_{by}(k-l). \tag{30}$$

Note that the cross-correlation functions $R_{yu}(\tau)$ of $y(t)$ and $u(t)$ and $R_{ye}(\tau)$ of $y(t)$ and $e(t)$ satisfy the relationship $R_{yu}(\tau)=0$ and $R_{ye}(\tau)=h_{by}(-\tau)$ (see Eqs. (A.4) and (A.7) in Appendix A). For $l>m_b$ the right-hand side of Eq. (30) equals zero, so that

$$\sum_{k=0}^{m_a} a_x(k)R_{xy}(k-l) = 0, \quad l \geqslant m_b+1. \tag{31}$$

Similarly, multiplying both sides of Eq. (24) by $x(t-l)$ and taking expectation on t, we can obtain the equation below:

$$\sum_{k=0}^{n_a} a_y(k)R_{xy}(l-k) = \sum_{k=0}^{n_b} b_y(k)h_{by}(k-l). \tag{32}$$

Note that the cross-correlation functions $R_{xv}(\tau)$ of $x(t)$ and $v(t)$ and $R_{xe}(\tau)$ of $x(t)$ and $e(t)$ satisfy the relationship $R_{xv}(\tau)=0$ and $R_{xe}(\tau)=h_{bx}(-\tau)$ (see Eqs. (A.3) and (A.6) of Appendix A). For $l>n_b$ the right-hand side of Eq. (32) also equals zero, so that

$$\sum_{k=0}^{n_a} a_y(k)R_{xy}(l-k) = 0, \quad l \geqslant n_b+1. \tag{33}$$

Eqs. (31) and (33) have the same form as the Yule–Walker (YW) equations for AR model or the modified Yule–Walker equations for ARMA model. Thus, the two AR coefficient series $a_x(j)$ and $a_y(j)$ can be computed in the same way as the YW equations. As $a_x(0)=1$ and $a_y(0)=1$ according to Eq. (7), a sufficient set of equations for the computation of the cross-correlation function sequence is $\mathbf{Ax}=\mathbf{y}$, where

$$\mathbf{x} = \{a_x(1), a_x(2), \ldots, a_x(m_a)\}^{\mathrm{T}}, \tag{34}$$

$$\mathbf{y} = \{-R_{xy}(-m_b-1), -R_{xy}(-m_b-2), \ldots, -R_{xy}(-m_b-n_e)\}^{\mathrm{T}}, \tag{35}$$

$$\mathbf{A} = \begin{bmatrix} R_{xy}(-m_b) & R_{xy}(-m_b+1) & \cdots & R_{xy}(m_a-m_b-1) \\ R_{xy}(-m_b-1) & R_{xy}(-m_b) & \cdots & R_{xy}(m_a-m_b-2) \\ \vdots & \vdots & & \vdots \\ R_{xy}(-m_b-n_e+1) & R_{xy}(-m_b-n_e+2) & \cdots & R_{xy}(m_a-m_b-n_e) \end{bmatrix}, \tag{36}$$

for Eq. (31),

$$\mathbf{x} = [a_y(1), a_y(2), \ldots, a_y(n_a)]^{\mathrm{T}}, \tag{37}$$

$$\mathbf{y} = [-R_{xy}(n_b+1), -R_{xy}(n_b+2), \ldots, -R_{xy}(n_b+n_e)]^{\mathrm{T}}, \tag{38}$$

$$\mathbf{A} = \begin{bmatrix} R_{xy}(n_b) & R_{xy}(n_b-1) & \cdots & R_{xy}(-n_a+n_b+1) \\ R_{xy}(n_b+1) & R_{xy}(n_b) & \cdots & R_{xy}(-n_a+n_b+2) \\ \vdots & \vdots & & \vdots \\ R_{xy}(n_b+n_e-1) & R_{xy}(n_b+n_e-2) & \cdots & R_{xy}(-n_a+n_b+n_e) \end{bmatrix} \tag{39}$$

for Eq. (33) and n_e is the number of equations.

If exact cross-correlations are given, one can solve $\mathbf{Ax} = \mathbf{y}$ as simultaneous equations where n_e is set to m_a or n_a. In practice, however, it is generally necessary to compute appropriate cross-correlation estimates from the given set of the time-series observations. Thus, to obtain the AR coefficients $a_x(j)$ and $a_y(j)$ with high accuracy, let n_e be set larger than m_a and n_a, then one can solve it in the least square sense. For large n_e, however, the solution of AR coefficient may be unstable, because the linear dependency of $\mathbf{Ax} = \mathbf{y}$ is getting lower. To avoid this difficulty, the singular value decomposition [26] is used in the numerical examples shown later.

4. Computation of auto-PSD based on ARMAMA model

In the previous section, the cross-PSD between two time series is derived. In this section, the auto-PSD of ARMAMA model will be derived under the condition that the cross-PSD is already obtained. Since the results concerning $x(t)$ and $y(t)$ have the same form, we will consider only $x(t)$ in the derivation below.

4.1. Derivation of general auto-PSD form

The auto-correlation function $R_{xx}(\tau)$ of $x(t)$ is given using Eq. (16) as

$$\begin{aligned} R_{xx}(\tau) &= E[x(t)\,x(t+\tau)] \\ &= \sum_{j=0}^{\infty}\sum_{k=0}^{\infty} h_{bx}(j)h_{bx}(k)E[e(t-j)e(t+\tau-k)] \\ &\quad + \sum_{j=0}^{\infty}\sum_{k=0}^{\infty} h_{dx}(j)h_{dx}(k)E[e_x(t-j)e_x(t+\tau-k)] \\ &= \sum_{j=0}^{\infty} h_{bx}(j)h_{bx}(j+\tau) + \sum_{j=0}^{\infty} h_{dx}(j)h_{dx}(j+\tau). \end{aligned} \tag{40}$$

Note that the inputs $e(t)$ and $e_x(t)$ are mutually independent.

Then the auto-PSD $S_{xx}(z^{-1})$ of $x(t)$ is given by

$$S_{xx}(z^{-1}) = \sum_{\tau=-\infty}^{\infty} R_{xx}(\tau) z^{-\tau}. \tag{41}$$

Since the impulse responses $h_{bx}(t)$ and $h_{dx}(t)$ are equal to zero for $t<0$, substitution of Eq. (40) into Eq. (41) leads to the equation below:

$$\begin{aligned} S_{xx}(z^{-1}) = & \sum_{j=0}^{\infty} \sum_{\tau=-j}^{\infty} h_{bx}(j) h_{bx}(j+\tau) z^{-\tau} \\ & + \sum_{j=0}^{\infty} \sum_{\tau=-j}^{\infty} h_{dx}(j) h_{dx}(j+\tau) z^{-\tau}. \end{aligned} \tag{42}$$

Let $k = j + \tau$ and substitute Eqs. (12) and (14) into Eq. (42), then the auto-PSD of Eq. (3) can be obtained as follows:

$$\begin{aligned} S_{xx}(z^{-1}) &= \sum_{j=0}^{\infty} \sum_{k=0}^{\infty} h_{bx}(j) h_{bx}(k) z^{-(k-j)} + \sum_{j=0}^{\infty} \sum_{k=0}^{\infty} h_{dx}(j) h_{dx}(k) z^{-(k-j)} \\ &= H_{bx}(z) H_{bx}(z^{-1}) + H_{dx}(z) H_{dx}(z^{-1}) \\ &= \frac{C_x(z) C_x(z^{-1}) B_x(z) B_x(z^{-1}) + D_x(z) D_x(z^{-1}) A_x(z) A_x(z^{-1})}{A_x(z) A_x(z^{-1}) C_x(z) C_x(z^{-1})}. \end{aligned} \tag{43}$$

4.2. Simple representation of auto-PSD without MA coefficient

The auto-PSD given by Eq. (43) can be rewritten using the cross-PSD representation given by Eq. (29), which is expressed without MA coefficients.

The numerator in Eq. (43) can be expressed as

$$\begin{aligned} & C_x(z) C_x(z^{-1}) B_x(z) B_x(z^{-1}) + D_x(z) D_x(z^{-1}) A_x(z) A_x(z^{-1}) \\ &= \sum_{i=0}^{m_c} \sum_{j=0}^{m_c} \sum_{k=0}^{m_b} \sum_{h=0}^{m_b} c_x(i) c_x(j) b_x(k) b_x(h) z^{-i+j+k-h} \\ &\quad + \sum_{i=0}^{m_d} \sum_{j=0}^{m_d} \sum_{k=0}^{m_a} \sum_{h=0}^{m_a} d_x(i) d_x(j) a_x(k) a_x(h) z^{-i+j+k-h} \\ &= \sum_{l=-(m_b+m_c)}^{m_b+m_c} \sum_{i=0}^{m_c} \sum_{j=0}^{m_c} \sum_{k=0}^{m_b} c_x(i) c_x(j) b_x(k) b_x(l-i+j+k) z^{-l} \\ &\quad + \sum_{l=-(m_a+m_d)}^{m_a+m_d} \sum_{i=0}^{m_d} \sum_{j=0}^{m_d} \sum_{k=0}^{m_a} + d_x(i) d_x(j) a_x(k) a_x(l-i+j+k) z^{-l} \end{aligned}$$

$$= \sum_{l=-M}^{M} \left(\sum_{i=0}^{m_c} \sum_{j=0}^{m_c} \sum_{k=0}^{m_b} c_x(i)c_x(j)b_x(k)b_x(l-i+j+k) + \sum_{i=0}^{m_d} \sum_{j=0}^{m_d} \sum_{k=0}^{m_a} + d_x(i)d_x(j)a_x(k)a_x(l-i+j+k) \right) z^{-l}. \quad (44)$$

Note that $h = l + i - j + k$; $c_x(j) = 0$ for $j < 0$ or for $m_c < j$; $d_x(j) = 0$ for $j < 0$ or for $m_d < j$, and M is the larger value of $m_b + m_c$ and $m_a + m_d$.

Let us introduce an instrumental variable $w(t)$ equivalent to the both sides of Eq. (8).

From the left-hand side of Eq. (8), the auto-correlation function $R_{ww}(\tau)$ of $w(t)$ can be expressed as

$$\begin{aligned} R_{ww}(l) &= E[w(t)\, w(t+l)] \\ &= \sum_{i=0}^{m_c} \sum_{j=0}^{m_c} \sum_{k=0}^{m_a} \sum_{h=0}^{m_a} c_x(i)c_x(j)a_x(k)a_x(h)E[x(t-j-k)\, x(t+l-i-h)] \\ &= \sum_{i=0}^{m_c} \sum_{j=0}^{m_c} \sum_{k=0}^{m_a} \sum_{h=0}^{m_a} c_x(i)c_x(j)a_x(k)a_x(h)R_{xx}(l-i+j+k-h), \end{aligned} \quad (45)$$

where $R_{xx}(\tau)$ is the auto-correlation function of $x(t)$.

Next, by using the right-hand side of Eq. (8), $R_{ww}(\tau)$ of $w(t)$ can also be expressed as

$$\begin{aligned} R_{ww}(l) &= E[w(t)\, w(t+l)] \\ &\quad \times \left(\sum_{i=0}^{m_c} \sum_{h=0}^{m_b} c_x(i)b_x(h)e(t+l-i-h) + \sum_{i=0}^{m_d} \sum_{h=0}^{m_a} d_x(i)a_x(h)e_x(t+l-i-h) \right) \\ &= \sum_{i=0}^{m_c} \sum_{j=0}^{m_c} \sum_{k=0}^{m_b} \sum_{h=0}^{m_b} c_x(i)c_x(j)b_x(k)b_x(h)E[e(t-j-k)e(t+l-i-h)] \\ &\quad + \sum_{i=0}^{m_d} \sum_{j=0}^{m_d} \sum_{k=0}^{m_a} \sum_{h=0}^{m_a} d_x(i)d_x(j)a_x(k)a_x(h)E[e_x(t-j-k)e_x(t+l-i-h)] \\ &= \sum_{i=0}^{m_c} \sum_{j=0}^{m_c} \sum_{k=0}^{m_b} c_x(i)c_x(j)b_x(k)b_x(l-i+j+k) \\ &\quad + \sum_{i=0}^{m_d} \sum_{j=0}^{m_d} \sum_{k=0}^{m_a} d_x(i)d_x(j)a_x(k)a_x(l-i+j+k). \end{aligned} \quad (46)$$

Then substituting Eq. (46) into Eq. (43) and using Eqs. (44) and (45), the alternative representation of auto-PSD in Eq. (21) can be obtained:

$$S_{xx}(z^{-1}) = \frac{\sum_{l=-M}^{M} R_{ww}(l)z^{-l}}{A_x(z)A_x(z^{-1})C_x(z)C_x(z^{-1})}. \quad (47)$$

Since $R_{ww}(l)$ can be computed for $l = -M, \ldots, M$, by using Eq. (45), the above auto-PSD could be evaluated without the use of MA coefficients.

4.3. Computation of AR coefficient

Multiplying both sides of Eq. (8) by $x(t-l)$ and taking expectation on t, we can obtain the equation below:

$$\sum_{j=0}^{m_c}\sum_{k=0}^{m_a} c_x(j)a_x(k)R_{xx}(j+k-l) = \sum_{j=0}^{m_c}\sum_{k=0}^{m_b} c_x(j)b_x(k)h_{bx}(j+k-l) + \sum_{j=0}^{m_d}\sum_{k=0}^{m_a} d_x(j)a_x(k)h_{dx}(j+k-l). \tag{48}$$

Note that the cross-correlation functions $R_{xe}(\tau)$ of $x(t)$ and $e(t)$ and $R_{xe_x}(\tau)$ of $x(t)$ and $e_x(t)$ satisfy the relationship $R_{xe}(\tau) = h_{bx}(-\tau)$ and $R_{xe_x}(\tau) = h_{dx}(-\tau)$. (See Eqs. (A.4) and (A.7) in Appendix A.) For $l > M$, the right-hand side of Eq. (48) equals zero, so that

$$\sum_{j=0}^{m_c}\sum_{k=0}^{m_a} c_x(j)a_x(k)R_{xx}(j+k-l) = 0, \quad l \geqslant M+1. \tag{49}$$

Here the AR coefficient $a_x(j)$ and auto-correlation function $R_{xx}(\tau)$ are already known, and $a_x(j)$ can be computed in the process of cross-PSD evaluation by using Eqs. (34)–(36), $R_{xx}(\tau)$ can be estimated from the observed output $x(t)$. Therefore, in Eq. (49), only the AR coefficients $c_x(j)$ are unknown. As $c_x(0) = 1$ in the definition of Eq. (7), a sufficient set of equations with $c_x(q)$ as unknowns are given from Eq. (49) as $[A_{pq}]\{x_q\} = \{y_p\}$, where

$$x_q = c_x(q), \tag{50}$$

$$y_p = -\sum_{k=0}^{m_a} a_x(k)R_{xx}(k-p), \tag{51}$$

$$A_{pq} = \sum_{k=0}^{m_a} a_x(k)R_{xx}(p-q-k), \quad (p = M+1-M+n_e,\ q = 1-m_c) \tag{52}$$

and n_e is the number of equations.

As described in the previous section, the AR coefficients $c_x(j)$ can be estimated as the solution of the equation $[A_{pq}]\{x_q\} = \{y_p\}$ in the least-square sense.

5. Comparison between ARMAMA model and multivariate models

The cross- and auto-PSD can be expressed by multivariate linear difference models as well as the ARMAMA model presented in the previous sections. For spectral estimation, however, the ARMAMA model can be handled more easily than the multivariate models due to the structural characteristics of the ARMAMA model, which can well separate correlated or uncorrelated components from two time records. To explain the applicability of the spectral estimation based on the ARMAMA model, an ARMAV model (autoregressive moving-average vector model) is

mentioned as an example of the multivariate models, and the structural difference between the ARMAMA model and the ARMAV model will be discussed.

Let $\mathbf{x}(t)$ and $\mathbf{e}(t)$ be observable output vectors and unobservable input vectors, the ARMAV model can be generally expressed as [22]

$$\mathbf{A}(z^{-1})\mathbf{x}(t) = \mathbf{B}(z^{-1})\mathbf{e}(t), \tag{53}$$

where $\mathbf{A}(z^{-1})$ and $\mathbf{B}(z^{-1})$ are the AR and the MA coefficient matrices, respectively. Then the PSD matrix of $\mathbf{x}(t)$ is given as [22]

$$\mathbf{S}_{\mathrm{ARMAV}}(z^{-1}) = (\mathbf{A}^{-1}(z)\mathbf{B}(z))\boldsymbol{\Sigma}_e(\mathbf{A}^{-1}(z^{-1})\mathbf{B}(z^{-1}))^{\mathrm{T}}, \tag{54}$$

where $\mathbf{S}_{\mathrm{ARMAV}}(z^{-1})$ is the PSD matrix of the ARMAV model; $\boldsymbol{\Sigma}_e$ is the PSD matrix of $\mathbf{e}(t)$; $\mathbf{A}^{-1}(z)$ denotes the inverse matrix of $\mathbf{A}(\mathbf{z})$. In the PSD matrix $\mathbf{S}_{\mathrm{ARMAV}}(z^{-1})$, the diagonal and the non-diagonal elements correspond to the auto- and cross-PSDs of $\mathbf{x}(t)$, respectively.

To simplify the discussion below on the structural difference of the PSD forms, a two-dimensional ARMAV model is introduced, which is given as

$$\sum_{k=0}^{m}\begin{bmatrix} a_{11}(k) & a_{12}(k) \\ a_{21}(k) & a_{22}(k) \end{bmatrix}\begin{Bmatrix} x(t-k) \\ y(t-k) \end{Bmatrix} = \sum_{j=0}^{n}\begin{bmatrix} b_{11}(k) & b_{12}(k) \\ b_{21}(k) & b_{22}(k) \end{bmatrix}\begin{Bmatrix} \varepsilon_x(t-j) \\ \varepsilon_y(t-j) \end{Bmatrix}, \tag{55}$$

where $x(t)$ and $y(t)$ are observable output sequences of two stationary processes; $\varepsilon_x(t)$ and $\varepsilon_y(t)$ are mutually independent white noise sequences with unit variances; $a_{pq}(k)$ and $b_{pq}(k)$ are the AR and the MA coefficients. By using the relation of Eqs. (53) and (54), the PSD matrix of the two-dimensional ARMAV model can be obtained:

$$\mathbf{S}_{\mathrm{ARMAV}}(z^{-1}) = \frac{1}{\Delta}\begin{bmatrix} A_{22}^* & -A_{12}^* \\ -A_{21}^* & A_{11}^* \end{bmatrix}\begin{bmatrix} B_{11}^* & B_{12}^* \\ B_{21}^* & B_{22}^* \end{bmatrix}\begin{bmatrix} B_{11} & B_{21} \\ B_{12} & B_{22} \end{bmatrix}\begin{bmatrix} A_{22} & -A_{21} \\ -A_{12} & A_{11} \end{bmatrix}, \tag{56}$$

where

$$\Delta = (A_{11}^*A_{22}^* - A_{12}^*A_{21}^*)(A_{11}A_{22} - A_{12}A_{21}), \tag{57}$$

$$A_{pq} = \sum_{k=0}^{n} a_{pq}(k)z^{-k}, \quad A_{pq}^* = \sum_{k=0}^{n} a_{pq}(k)z^{k} \ \ (p = 1,2;\ q = 1,2), \tag{58}$$

$$B_{pq} = \sum_{k=0}^{n} b_{pq}(k)z^{-k}, \quad B_{pq}^* = \sum_{k=0}^{n} b_{pq}(k)z^{k} \ \ (p = 1,2;\ q = 1,2). \tag{59}$$

When the AR and MA coefficients of $a_{pq}(k)$ and $b_{pq}(k)$ can be determined by some scheme [20,22,23], the auto- and cross-PSDs are numerically computed by Eq. (56), which are, respectively, given as the diagonal and the non-diagonal elements of $\mathbf{S}_{\mathrm{ARMAV}}(z^{-1})$. However, it is difficult to give analytical consideration on Eq. (56) because of its complex expression. For instance, the auto- and cross-PSD expressions given by Eq. (56) have the same denominator as Δ; therefore, all of the auto- and cross-PSDs have the same poles, which are determined from the solution of $\Delta = 0$. This means one cannot analytically separate correlated or uncorrelated components from two time records. This analytical difficulty is common to all types of multivariate linear difference models.

On the other hand, the auto- and cross-PSDs given by the ARMAMA model, as shown in Eqs. (29) and (47), are simple and one can give a theoretical consideration of spectral analysis more easily, as stated below. In practice, the physical parameters can be directly obtained from the coefficients of the PSDs' expressions, when the relations of both physical and ARMAMA models have been formulated. Moreover, the difference of each denominator for the auto- and cross-PSDs helps spectral analysis for correlated two time records, that is, the poles given from $A_x(z)A_y(z^{-1}) = 0$ correspond to the correlated signals, whereas the poles given from $C_x(z)C_x(z^{-1}) = 0$ correspond to the uncorrelated signals.

6. Numerical examples

To illustrate the application on the spectral analysis procedure presented in the paper, two numerical examples are shown. In both examples, sample sequences are simulated as measured records of mechanical vibration response with colored noises. In the first example (Example 1), a two degree-of-freedom (2-dof) coupled system is considered; i.e., the responses of each mass have two common sinusoidal components. In the second example (Example 2) two single-dof systems driven by a common input are treated; i.e., the responses have a different sinusoidal component to one another.

To confirm the accuracy of the cross- and the auto-PSD estimates for these examples, the spectral shapes of the PSDs obtained by the present procedure will be compared with theoretical ones. Moreover, the authors shall evaluate the eigen properties of both vibration systems and the colored noise (which has eigen frequency) included in the cross- and auto-PSD estimates.

In the application of the present procedure to these examples, the singular value decomposition (SVD) procedure [26] is used in the estimation of the AR parameters $a_x(j)$, $a_y(j)$, $c_x(j)$ and $c_y(j)$, where the small singular values are neglected when the ratio of the singular value to the largest one is less than $\frac{1}{100}$. The orders of ARMAMA are fixed as $m_i = n_i = m$ $(i = a, b, c, d)$, and the number of the YW equations is set to $n_e = 5m$.

6.1. Example 1

6.1.1. Simulation model

The governing equations in this example are given as follows:

System:

$$\begin{Bmatrix} \ddot{p}(t) \\ \ddot{q}(t) \end{Bmatrix} + \frac{\pi}{5}\begin{bmatrix} 5 & -2 \\ -2 & 2 \end{bmatrix}\begin{Bmatrix} \dot{p}(t) \\ \dot{q}(t) \end{Bmatrix} + 100\pi^2\begin{bmatrix} 5 & -2 \\ -2 & 2 \end{bmatrix}\begin{Bmatrix} p(t) \\ q(t) \end{Bmatrix} = -\begin{Bmatrix} e_1(t) \\ e_1(t) \end{Bmatrix}. \tag{60}$$

Noises:

$$\ddot{\varepsilon}_p(t) + 0.12\pi\dot{\varepsilon}_p(t) + 144\pi^2\varepsilon_p(t) = -e_2(t), \tag{61}$$

$$\ddot{\varepsilon}_q(t) + 0.08\pi\dot{\varepsilon}_q(t) + 64\pi^2\varepsilon_q(t) = -e_3(t). \tag{62}$$

Observations:

$$x(t) = (\ddot{p}(t) + e_1(t)) + (\ddot{\varepsilon}_p(t) + e_2(t)), \tag{63}$$

$$y(t) = (\ddot{q}(t) + e_1(t)) + (\ddot{\varepsilon}_q(t) + e_3(t)), \tag{64}$$

where $p(t)$ and $q(t)$ are relative displacement responses of the 2-dof vibration system to the ground; $\varepsilon_p(t)$ and $\varepsilon_q(t)$ are colored noises; $x(t)$ and $y(t)$ are observed outputs; $e_1(t)$, $e_2(t)$ and $e_3(t)$ are the mutually independent white noises with zero mean and unit variance; $\dot{}$ and $\ddot{}$ denote the first and the second derivatives with respect to time t. Fig. 2 shows the vibration system and its observation models of the example. The physical meaning of the model is that the 2-dof system is driven by the ground acceleration $e_1(t)$ and the observed absolute acceleration responses of $x(t)$ and $y(t)$ are $\ddot{p}(t) + e_1(t)$ and $\ddot{q}(t) + e_1(t)$, which are contaminated by the colored noises $\ddot{\varepsilon}_p(t) + e_2(t)$ and $\ddot{\varepsilon}_p(t) + e_3(t)$, respectively.

In the practical sense, the 2-dof system and the colored noises can be identical to an unknown vibration system of interest and the local mechanical noises due to member vibrations or artificial mechanical sources, respectively. Then the significant peaks of cross-PSD between two records can represent the common sinusoidal components, that is, the peaks can be considered as the modal characteristics of the unknown system.

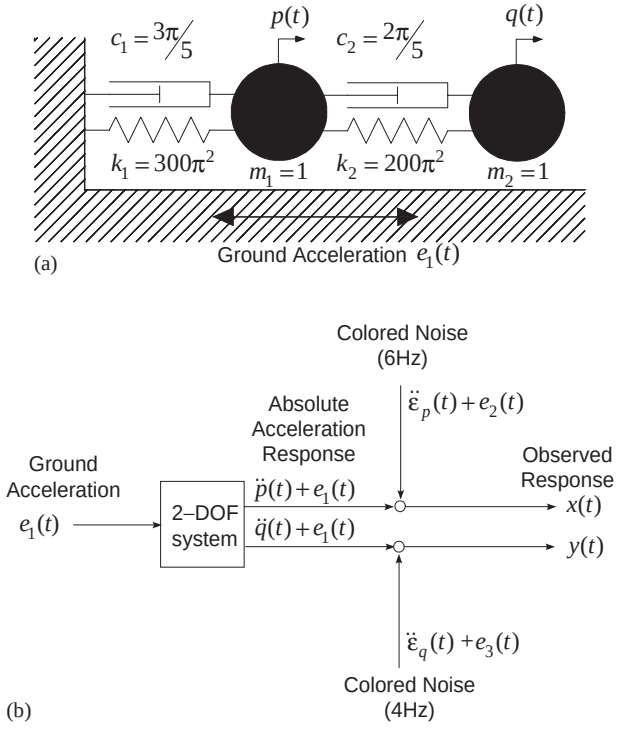

Fig. 2. Simulation model of Example 1: (a) system model; (b) observation model.

Theoretical eigenproperties of the model are shown in Table 1. Here, the relationship between the jth complex eigenvalue λ_j and the eigenfrequency f_j or the damping factor h_j is defined as [17]

$$2\pi f_j = |\lambda_j| \operatorname{sign}[\operatorname{Im}(\lambda_j)], \tag{65}$$

$$h_j = \cos \arg \lambda_j. \tag{66}$$

Here, $\operatorname{Im}(z)$ denotes the imaginary part of an complex number z; sign[·] denotes signum function which is defined as

$$\operatorname{sign}[\alpha] = \begin{cases} 1, & (\alpha \geqslant 0), \\ -1, & (\alpha < 0). \end{cases} \tag{67}$$

arg z denotes the argument of a complex number z. Using Eqs. (65) and (66), a pair of conjugate complex λ_j and λ_j^* is translated into f_j and $-f_j$ in eigen frequency, and into the same value h_j in damping factor.

The outputs $x(t)$ and $y(t)$ have the two modal components whose eigen frequencies are 5 Hz and $5\sqrt{6}$ (≈ 12.25) Hz in common. Additionally, the first modal component and the two colored noises are closely spaced in frequency, while the second modal component and the noises are widely spaced.

Eqs. (60)–(62) are solved by numerical integration (herein by Runge–Kutta–Gill method), where the initial conditions are set $p(0) = \dot{p}(0) = 0$, $q(0) = \dot{q}(0) = 0$, $\varepsilon_p(0) = \dot{\varepsilon}_p(0) = 0$ and $\varepsilon_q(0) = \dot{\varepsilon}_q(0) = 0$, and the time interval $\Delta t = 0.005$ s. After that, the samples of output sequences given by Eqs. (63) and (64) are obtained by resampling them with the time interval $\Delta t = 0.02$ s.

6.1.2. *Spectral estimation results*

Fig. 3 shows the cross-PSD estimates $S_{xy}(f)$ obtained by the present procedure with the order of the ARMAMA model $m = 2, 4, 10$, and also obtained by the FFT, where the number of sample data $N = 2^{14}$. Here, the cross-PSD by the FFT is described as the average of 16 estimates; i.e., the number of each small sample is set to 2^{10}.

Comparing the cross-PSD estimates by the present procedure with the order of the ARMAMA model, shown in Fig. 3(a)–(c), the cross-PSD with $m = 4$ shows the best agreement with the

Table 1
The eigenvalues and eigenvectors of Example 1

	Eigenvalues		Eigenvectors $\{\phi_{pj}, \phi_{qj}\}$
	Freq. (Hz)	Damp.	
System			
1st mode	5	1/100	$\{1/2, 1\}$
2nd mode	$5\sqrt{6}$	$\sqrt{6}/100$	$\{-2, 1\}$
Noises			
ε_p	4	5/1000	—
ε_q	6	5/1000	—

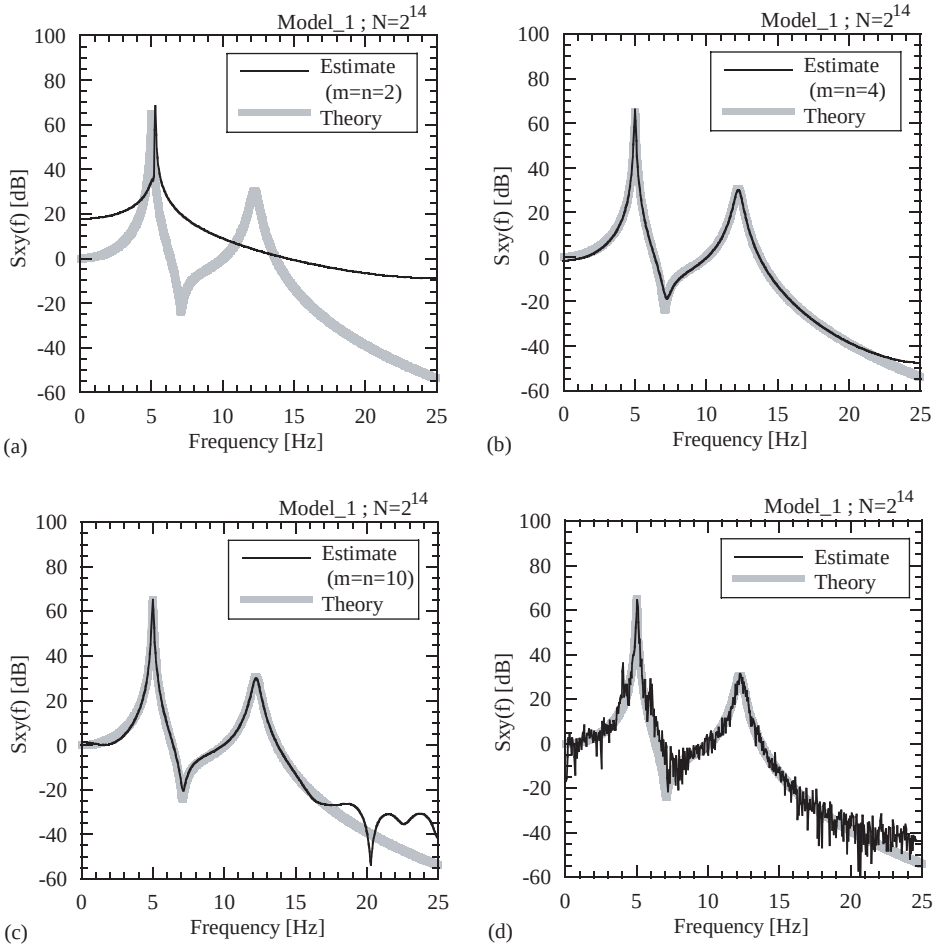

Fig. 3. Cross-PSD estimates of Example 1, where the number of sample data $N = 2^{14}$. Proposed method with the order of ARMAMA model: (a) $m = 2$, (b) $m = 4$, (c) $m = 10$, (d) the average over 16 estimates by the FFT method.

theoretical spectrum in wide frequency range, and the cross-PSD with $m = 10$ also agrees well with the theoretical one in amplitude range larger than -20 dB. In contrast with these estimates, the cross-PSD with $m = 2$ in Fig. 3(a) is poorly estimated.

Since the poles appear as a pair of conjugates in vibration theory, the 2-dof vibration system in Eq. (60) has four poles. Thus, for the best cross-PSD estimate shown in Fig. 3(b), the order of the ARMAMA model equals the number of poles in the cross-PSD between $x(t)$ and $y(t)$. Therefore, from Fig. 3(a)–(c) it can be stated that the order of the ARMAMA model should be larger than the number of poles in the cross-PSD, to obtain a better cross-PSD estimate. As shown in Fig. 3(c), the larger order of the ARMAMA model seems to distort the cross-PSD estimate in the very low amplitude range: e.g., in amplitudes lower than -20 dB in the figure, however, the part of the cross-PSDs in the higher amplitude range will not be distorted, which often play an important role in wide engineering field.

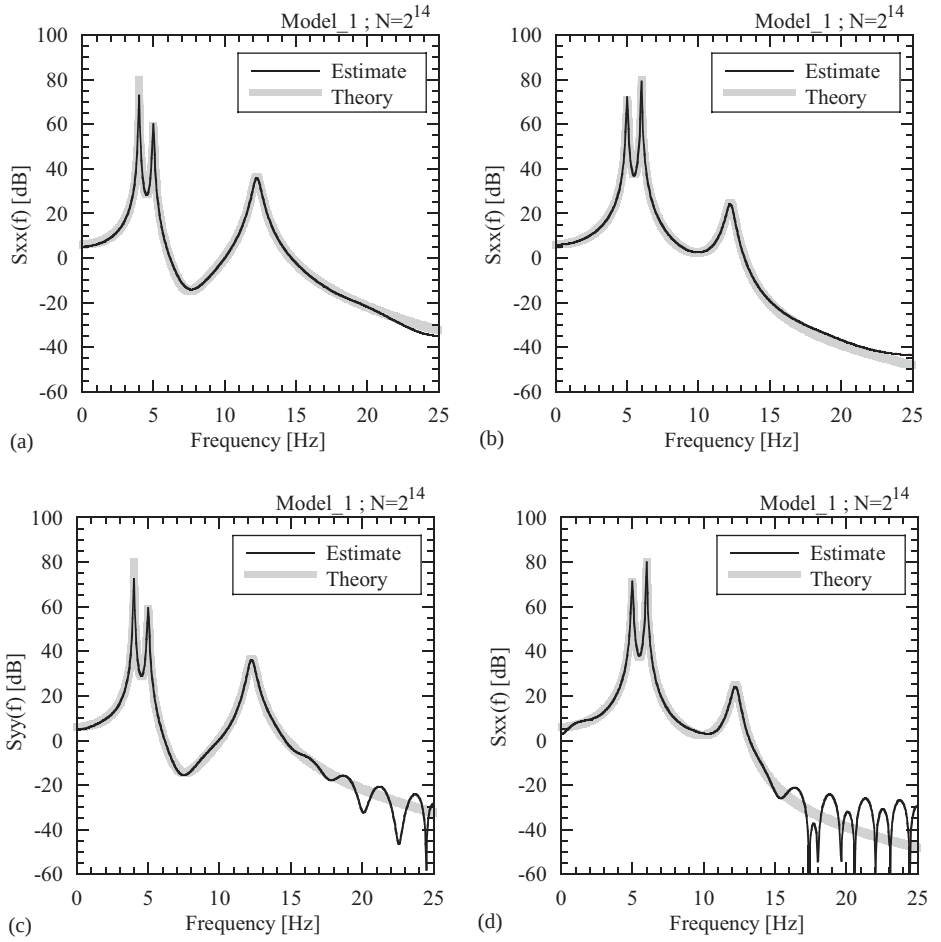

Fig. 4. Auto-PSD estimates by the proposed method in Example 1, where the number of sample data $N = 2^{14}$. The auto-PSD of (a) $x(t)$ and (b) $y(t)$ with the order of ARMAMA model $m = 4$, the auto-PSD of (c) $x(t)$ and (d) $y(t)$ with the order of ARMAMA model $m = 10$.

On the other hand, the cross-PSD estimate by a conventional method of the FFT, as shown in Fig. 3(d), has two small peaks around the resonance peak at 5 Hz. By using the FFT the two peaks at 4 and 6 Hz do not vanish perfectly, which are caused by the additional colored noises, whereas in the cross-PSD by the proposed procedure there is no peak of the additional colored noises.

Fig. 4 shows the associate auto-PSD estimates $S_{xx}(f)$ and $S_{yy}(f)$ by the present procedure with $m = 4$ and 10, which also describes the theoretical spectra. As shown in Fig. 4(a) and (b), the auto-PSD estimates $S_{xx}(f)$ and $S_{yy}(f)$ show the best agreement with the theoretical spectrum in a wide frequency range, when the order of the ARMAMA model is equal to $m = 4$. Also, two auto-PSD estimates $S_{xx}(f)$ and $S_{yy}(f)$ with $m = 10$, shown in Fig. 4(c) and (d), agree with the theoretical one, except lower amplitude range than -20 dB.

According to these results on the cross- and auto-PSD estimates, by using the proposed procedure, both correlated signal and uncorrelated noises can be well-separately identified from the two output sequences even when the signal and noises are closely spaced.

6.1.3. Eigenproperty estimation results

The advantage of parametric spectral estimations such as the present procedure is that physical parameters can directly be obtained from coefficients of the spectral estimates when the relationships between the physical parameters and the spectral estimates have been formulated. To investigate the aforementioned result of the cross- and auto-PSDs in more detail, the eigenproperties estimated from the coefficients of cross- and auto-PSDs will be confirmed. Before investigating in detail, the authors will show the procedure where the eigen properties can be estimated from the cross- and auto-PSDs shown in Fig. 3(c) and Fig. 4(c) and (d).

The eigenproperty estimates associated with $A_x(z) = 0$ and $A_y(z^{-1}) = 0$ are shown in Tables 2 and 3. Here, the poles are translated into the eigenfrequencies and damping factors by Eqs. (65) and (66); the residues γ_{xy} and β_{xy} are calculated from the cross-PSD estimate $S_{xy}(z^{-1})$ associated with the pole in $A_x(z) = 0$ and in $A_y(z^{-1}) = 0$; the residues γ_{xx} and β_{yy} are calculated from the auto-PSD estimates $S_{xx}(z^{-1})$ and $S_{yy}(z^{-1})$.

Comparing Tables 2 and 3 with Table 1, the No. 1–4 eigenparameter estimates seem to be related to the vibration system. For the No. 5–10 estimates, on the other hand, the physical meaning cannot be clear. When the order of the ARMAMA model is set to be larger than the true order of the physical model (as in this example, where the order of the mechanical system equals 4, and the order of the ARMAMA model is set to 10), not only substantial poles but also spurious poles appear. However, the substantial poles such as the No. 1–4 estimates appear as a pair of

Table 2
Eigenparameter estimates obtained from $A_x(z)$ in Example 1, where the number of sample data is $N = 2^{14}$; the order of ARMAMA model is $m = 10$

No.	Pole		Residue		γ_{xy}/γ_{xx}	
	Frequency (Hz)	Damping (%)	$\lvert\gamma_{xy}\rvert$ (gal^2)	$\lvert\gamma_{xx}\rvert$ (gal^2)	Absolute (·)	Phase (deg)
1	4.99	1.00	291.5	582.7	0.500	−1.7
2	−4.99	1.00	291.5	582.7	0.500	1.7
3	12.25	2.55	30.4	15.8	1.929	−170.3
4	−12.25	2.55	30.4	15.8	1.929	170.3
5	18.22	13.05	1.0	43.4	0.024	−144.2
6	−18.22	13.05	1.0	43.4	0.024	144.2
7	23.10	14.36	2.2	532.4	0.004	−107.2
8	−23.10	14.36	2.2	532.4	0.004	107.2
9	2.28	100.00	5.0	38.1	0.131	0.0
10	36.52	72.90	13.3	13954.2	0.000	0.0

Here, γ_{xy} and γ_{xx} are the residues of the cross-PSD $S_{xy}(z^{-1})$ and the auto-PSD $S_{xx}(z^{-1})$, which correspond to the poles in $A_x(z) = 0$.
(gal) = (cm/s^2): unit of acceleration.

Table 3
Eigen parameter estimates obtained from $A_y(z^{-1})$ in Example 1, where the number of sample data is $N = 2^{14}$; the order of ARMAMA model is $m = 10$

No.	Pole		Residue		β_{yy}/β_{xy}	
	Frequency (Hz)	Damping (%)	$\lvert\beta_{xy}\rvert$ (gal^2)	$\lvert\beta_{yy}\rvert$ (gal^2)	Absolute (·)	Phase (deg)
1	4.99	0.98	294.4	148.1	0.503	−2.2
2	−4.99	0.98	294.4	148.1	0.503	2.2
3	12.24	2.47	30.3	60.9	2.007	−171.8
4	−12.24	2.47	30.3	60.9	2.007	171.8
5	18.21	13.04	3.3	18.6	5.674	−60.9
6	−18.21	13.04	3.3	18.6	5.674	60.9
7	23.10	14.33	8.2	63.6	7.749	−17.5
8	−23.10	14.33	8.2	63.6	7.749	17.5
9	−2.27	100.00	9.7	10.3	1.068	180.0
10	36.02	71.99	699.3	2637.5	3.772	0.0

Here, β_{xy} and β_{yy} are the residues of the cross-PSD $S_{xy}(z^{-1})$ and the auto-PSD $S_{yy}(z^{-1})$, which correspond to the poles in $A_y(z^{-1}) = 0$.
(gal) = (cm/s^2): unit of acceleration.

conjugates, and the associated residues γ_{xy} and β_{xy} have significantly large absolute value; therefore, by using these characteristics of substantial poles, one can eliminate the spurious poles from all the poles in practice.

Similarly, Table 4 shows the eigenproperty estimates associated with $C_x(z^{-1})$ and $C_y(z^{-1})$. Here, the residues ζ_x and ζ_y are calculated from the auto-PSD estimates $S_{xx}(z^{-1})$ and $S_{yy}(z^{-1})$, which correspond to the poles in $C_x(z^{-1}) = 0$ and $C_y(z^{-1}) = 0$. Comparing Table 4 with Table 1, the No. 1 and 2 estimates of $C_x(z^{-1})$ and $C_y(z^{-1})$ seem to be related to the additional noises. The poles of these estimates appear as a pair of conjugates, and the associated residues become rather large in absolute value. The characteristics for the pole and residue tend to be similar to those in $A_x(z) = 0$ and $A_y(z^{-1}) = 0$. Therefore, one can also identify the properties of considerable noises in the same manner as in $A_x(z)$ and $A_y(z^{-1})$.

According to the above considerations, accuracy of the eigenproperty estimates is investigated with the length of the sample data, when the order of the ARMAMA model is fixed to $m = 10$. Tables 5 and 6 show eigenproperty estimates of the vibration system and the noises obtained by the cross- and auto-PSDs with the different lengths of sample data. Here, in Table 5 the estimates of poles or residues from $A_x(z) = 0$ and $A_y(z^{-1}) = 0$ are shown at the upper and lower rows in the cells, respectively. As shown in the table, the estimates for each eigenparameter converge to the true values with increasing data length. In the practical sense, the length of sample data is required over 2^{14} or more for the accurate eigenproperty estimation.

In turn, an influence of the eigenproperty estimates on the order of the ARMAMA model will be investigated, when the length of sample data is fixed to $N = 2^{14}$. Fig. 5 shows stabilization diagrams [27], where the eigenproperty estimates of the 2-dof system change with changing the order of the ARMAMA model m. As shown in the figure, each eigenproperty estimate rapidly converges with increasing the order m, and equals the true value when the order m is set to over 4.

Table 4
Eigen parameter estimates obtained from $C_x(z^{-1})$ and $C_y(z^{-1})$ in Example 1, where the number of sample data is $N = 2^{14}$; the order of ARMAMA model is $m = 10$

No.	$C_x(z^{-1})$			$C_y(z^{-1})$		
	Pole		Residue $\lvert\zeta_x\rvert$ (gal^2)	Pole		Residue $\lvert\zeta_y\rvert$ (gal^2)
	Frequency (Hz)	Damping (%)		Frequency (Hz)	Damping (%)	
1	6.00	0.46	1055.6	3.99	0.67	472.1
2	−6.00	0.46	1055.6	−3.99	0.67	472.1
3	11.92	16.60	10.4	10.25	15.49	1.2
4	−11.92	16.60	10.4	−10.25	15.49	1.2
5	17.05	15.92	54.6	15.28	12.40	7.2
6	−17.05	15.92	54.6	−15.28	12.40	7.2
7	22.34	14.99	504.8	20.20	10.06	13.5
8	−22.34	14.99	504.8	−20.20	10.06	13.5
9	−1.12	100.00	13.2	5.33	100.00	62.8
10	−26.22	30.14	3222.8	25.09	8.27	16.8

Here, ζ_x and ζ_y are the residues of the auto-PSD $S_{xx}(z^{-1})$ and $S_{yy}(z^{-1})$, which correspond to the poles in $C_x(z^{-1}) = 0$ and $C_y(z^{-1}) = 0$, respectively.
(gal) = (cm/s^2): unit of acceleration.

Therefore, the present procedure gives the accurate estimate when the order is selected to over the number of the poles in the cross-PSD. Practically, the true number of poles in a cross-PSD may not be known; however, the eigenproperties can be determined from the estimates by the present procedure, which are constant with successive orders of ARMAMA model.

6.2. Example 2

6.2.1. Simulation model

The equations of a vibration system are given as

System:

$$\begin{Bmatrix} \ddot{p}(t) \\ \ddot{q}(t) \end{Bmatrix} + \frac{\pi}{5}\begin{bmatrix} 1 & 0 \\ 0 & 6 \end{bmatrix}\begin{Bmatrix} \dot{p}(t) \\ \dot{q}(t) \end{Bmatrix} + 100\pi^2\begin{bmatrix} 1 & 0 \\ 0 & 6 \end{bmatrix}\begin{Bmatrix} p(t) \\ q(t) \end{Bmatrix} = -\begin{Bmatrix} e_1(t) \\ e_1(t) \end{Bmatrix}. \tag{68}$$

The same equations for noises and observations are used as in Example 1. The samples of output sequences $x(t)$ and $y(t)$ are generated by the same procedure as in Example 1.

Fig. 6 shows the vibration system and its observation models of the example. Theoretical eigenproperties of the model are shown in Table 7. In this example, the two outputs have no common modal components; i.e., each output $x(t)$ and $y(t)$ has only one modal component whose eigenfrequency is 5 Hz and $5\sqrt{6}$ (≈ 12.25) Hz, respectively. In a similar way as in Example 1, the first modal component and the dominant frequency of two colored noises are closely spaced in frequency range, while the second modal component and the dominant frequency of the noises are widely spaced.

Table 5
Estimated eigenproperties for the frequencies f_1, f_2, the damping coefficients h_1, h_2 and the modal amplitude ratio $\phi_{p1}/\phi_{q1}, \phi_{p2}/\phi_{q2}$ in Example 1, where the order of ARMAMA model is $m = 10$

N	1st Mode			2nd Mode		
	f_1 (Hz)	h_1 (%)	$\lvert\gamma_{xy}/\gamma_{xx}\rvert$ (·)	f_2 (Hz)	h_2 (%)	$\lvert\beta_{xy}/\beta_{yy}\rvert$ (·)
2^{10}	5.19	6.14	0.525	12.42	3.46	2.537
	4.78	5.54	0.421	12.46	3.60	1.711
2^{12}	4.99	1.60	0.507	12.27	3.51	1.769
	5.01	1.44	0.536	12.27	3.43	1.970
2^{14}	4.99	1.00	0.500	12.25	2.55	1.929
	4.99	0.99	0.503	12.24	2.47	2.007
2^{16}	5.00	1.01	0.501	12.24	2.48	2.011
	5.00	1.00	0.501	12.25	2.40	1.989
2^{18}	5.00	1.00	0.500	12.25	2.46	1.998
	5.00	1.00	0.501	12.25	2.45	1.994
2^{20}	5.00	1.00	0.503	12.25	2.47	1.996
	5.00	1.00	0.501	12.25	2.47	1.997
True	5.00	1.00	0.500	12.25	2.45	2.000

The upper and lower values in each cell of each row are obtained from $A_x(z) = 0$ and $A_y(z^{-1}) = 0$ in the each dataset, respectively.
N denotes the number of the data length.
$|\beta_{xy}/\beta_{yy}|$ and $|\gamma_{xy}/\gamma_{xx}|$ denote the absolute values of the residue ratio of the cross-PSD to the auto-PSD.

Table 6
Estimated noise properties for the frequencies f_p, f_q and the damping coefficients h_p, h_q in Example 1, where the order of ARMAMA model is $m = 10$

N	Noise ε_p		Noise ε_q	
	f_p (Hz)	h_p (%)	f_q (Hz)	h_q (%)
2^{10}	6.00	1.19	4.01	0.57
2^{12}	6.00	0.44	4.00	0.92
2^{14}	6.00	0.46	3.99	0.67
2^{16}	6.00	0.56	4.00	0.62
2^{18}	6.00	0.52	4.00	0.52
2^{20}	6.00	0.49	4.00	0.51
True	6.00	0.50	4.00	0.50

N denotes the number of the data length.

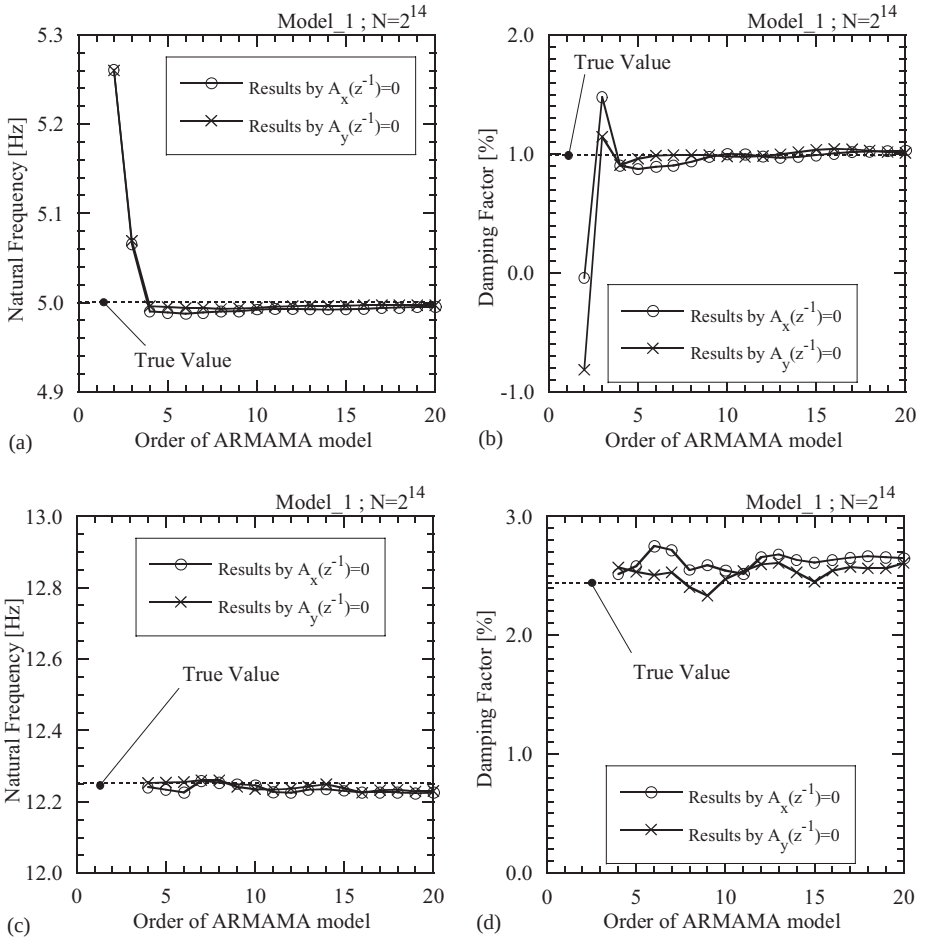

Fig. 5. Comparisons of eigenparameter estimates of Example 1 with the order of ARMAMA model, where the number of sample data $N = 2^{14}$: (a) The 1st frequency estimates, (b) the 1st damping factor estimates, (c) the 2nd frequency estimates, and (d) the 2nd damping factor estimates.

6.2.2. *Spectral estimation results*

Fig. 7 shows the cross-PSD estimates $S_{xy}(f)$ obtained by the present procedure and the FFT, where the lengths of sample data are $N = 2^{14}$, 2^{16} and 2^{18}, respectively. In the use of the FFT, the number of the sample in each estimate is 2^{10}, and the cross-PSDs by the FFT are given as the average of 16 (= 2^4), 64 (= 2^6) and 256 (= 2^8) estimates in each case.

As shown in Fig. 7(a), (c) and (e), it is apparent that the proposed procedure gives good results when the data length of the sample sequences is large enough . It is because the cross-correlation function can be well estimated from the long sample data, shown in Fig. 8.[2]

Similarly to the present procedure, by the FFT the cross-PSD accuracy increases with larger length of sample data, shown in Fig. 7(b), (d) and (f). Comparing both cross-PSD estimates by the

[2]The poles in $A_x(z) = 0$ and in $A_y(z^{-1}) = 0$ are estimated from $R_{xy}(t)$ in $t<0$ and in $t>0$, respectively.

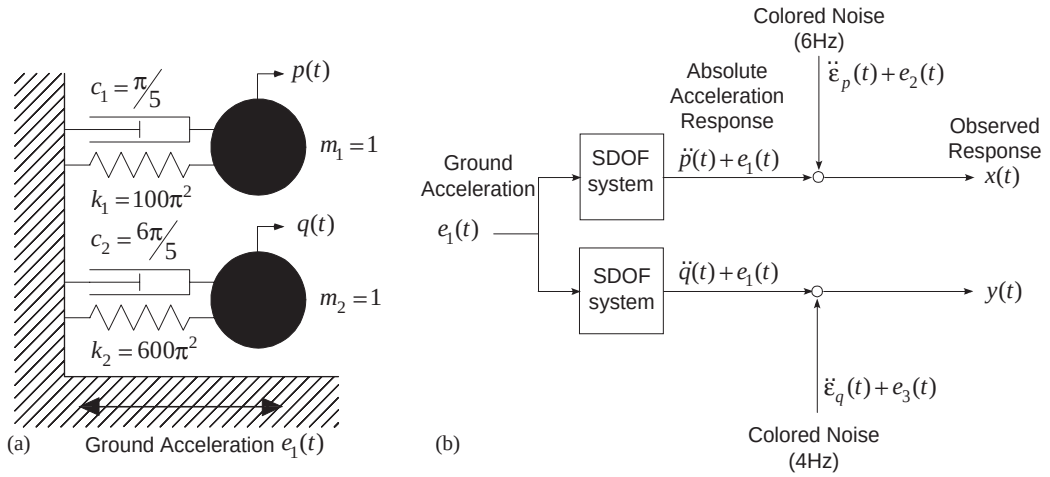

Fig. 6. Simulation model of Example 2: (a) system model, (b) observation model.

Table 7
The eigenvalues and eigenvectors of Example 2

	Eigenvalues		Eigenvectors $\{\phi_p, \phi_q\}$
	Freq. (Hz)	Damp.	
System			
1st mode	5	1/100	$\{1, 0\}$
2nd mode	$5\sqrt{6}$	$\sqrt{6}/100$	$\{0, 1\}$
Noises			
ε_p	4	5/1000	—
ε_q	6	5/1000	—

present procedure and the FFT within the same length of sample data, the present procedure gives better cross-PSD estimates to remove the additional noise peaks than the FFT method: e.g., according to Fig. 7 the noise peaks in (c) or (e) are lower than those in (d) or (f).

As shown in Fig. 9, the auto-PSD estimates $S_{xx}(f)$ and $S_{yy}(f)$ are also in good agreement with the theoretical spectra, associated with the cross-PSD obtained from the sample of the data length $N = 2^{16}$.

6.2.3. *Eigenproperty estimation results*

Furthermore, to investigate the accuracy of the cross- and auto-PSD estimates by the present procedure, the eigenproperties of the vibration system and the noises are evaluated as shown in Tables 8 and 9. Here, the γ_{xy}/γ_{xx} and β_{xy}/β_{yy} are the residue ratios of the cross-PSD to the auto-PSD, whose theoretical values are solved by Eqs. (68), (61)–(64) analytically. The eigenproperty estimates converge to the true values as shown in Table 7 with increasing length of the sample data. In practical sense, the number of the sample data required is over 2^{16} or more, which is

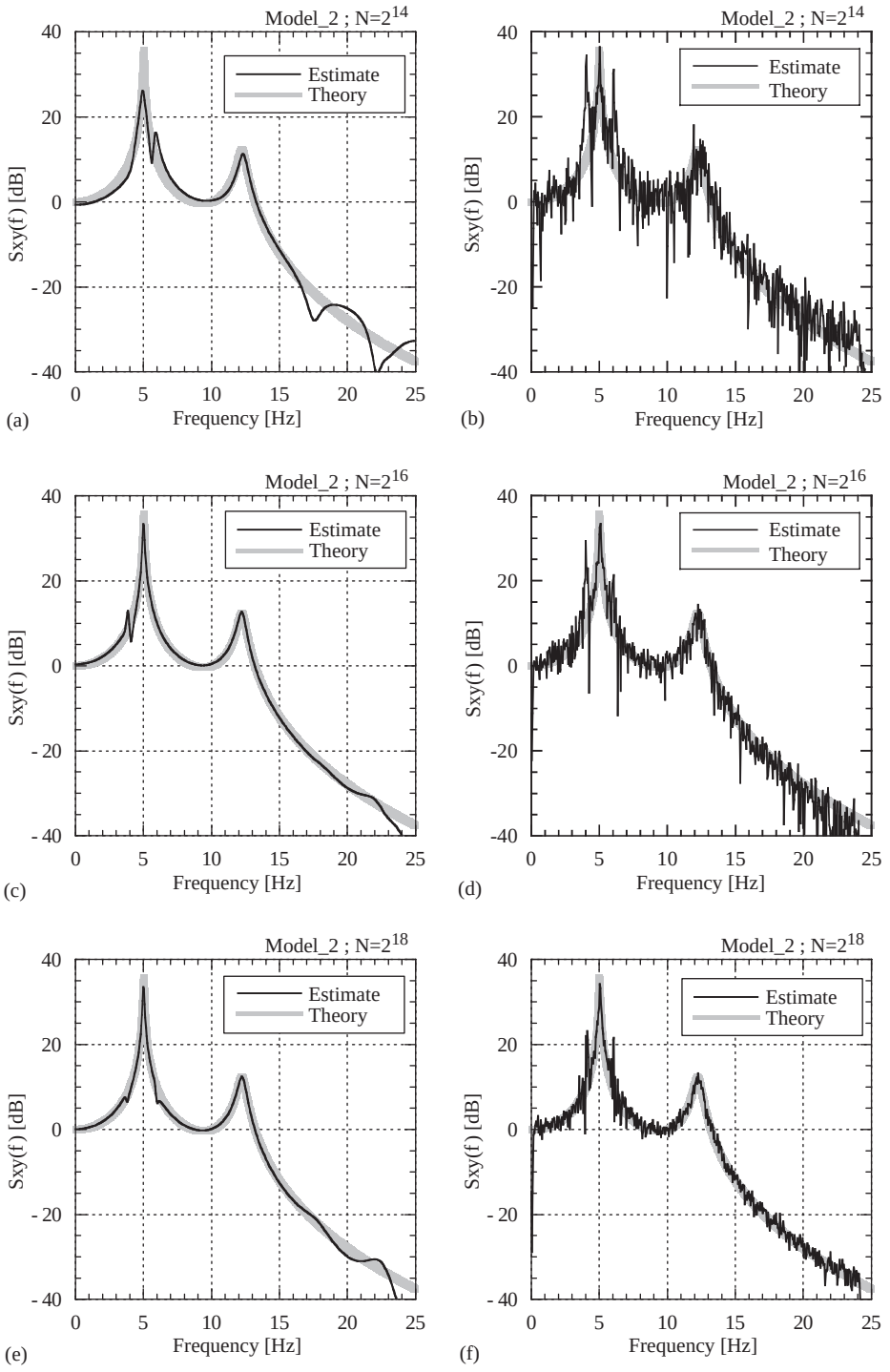

Fig. 7. Cross-PSD estimates of Example 2. Proposed method estimates with the order of ARMAMA model $m = 10$, where the number of the sample data: (a) $N = 2^{14}$, (c) $N = 2^{16}$, (e) $N = 2^{18}$. FFT method estimates where the number of the sample data: (b) $N = 2^{14}$, (d) $N = 2^{16}$, (f) $N = 2^{18}$.

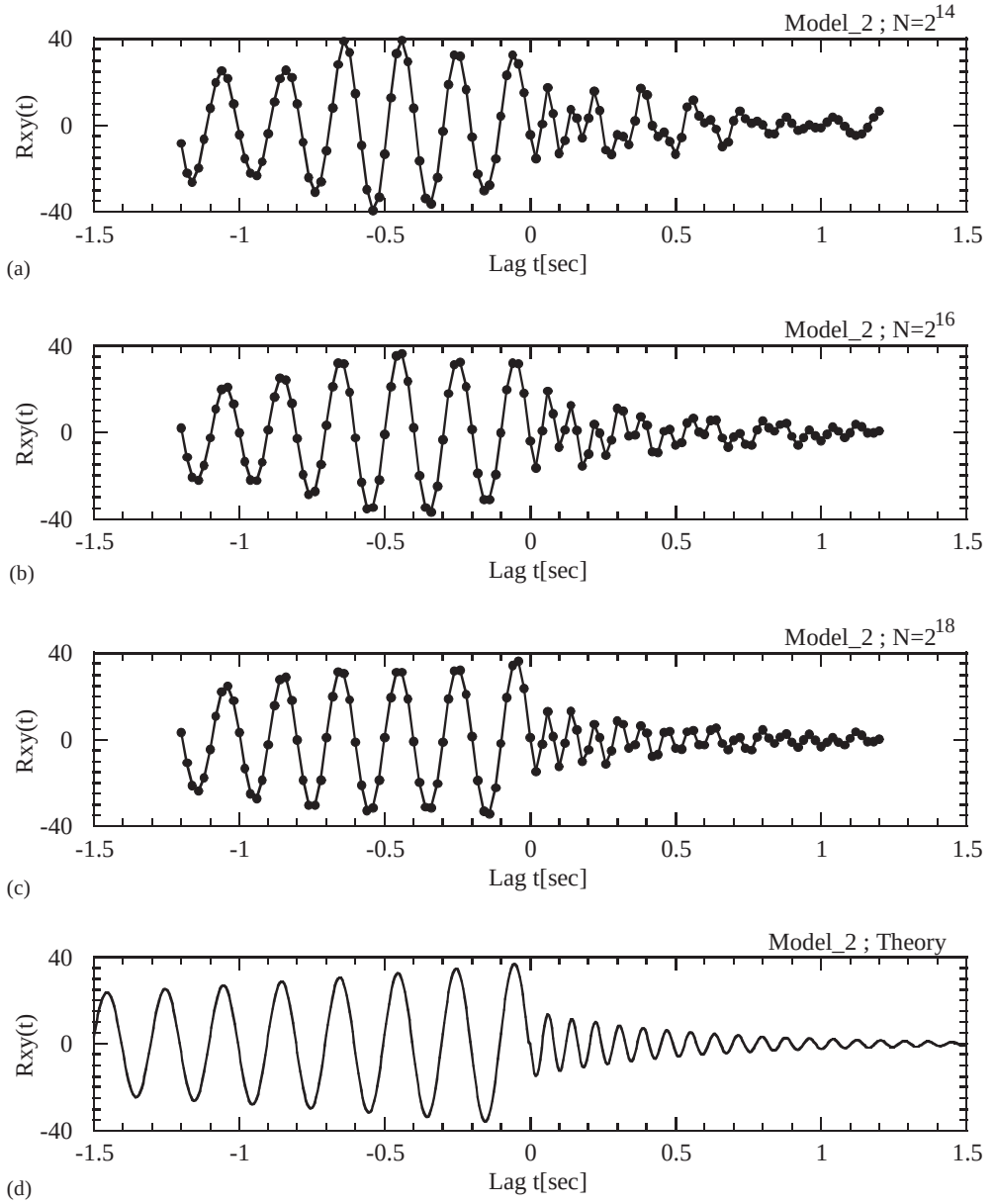

Fig. 8. Cross-correlation functions of $x(t)$ and $y(t)$ in Example 2, used for the cross-spectrum estimates. The number of the sample data is (a) $N = 2^{14}$, (b) $N = 2^{16}$, (c) $N = 2^{18}$ and (d) $N = \infty$ (in theory).

larger than that in Example 1. The reason is that in Example 2 the two outputs $x(t)$ and $y(t)$ have no common sinusoidal components; i.e., in the frequency range near 5 Hz $x(t)$ has the dominant component while $y(t)$ has no dominant component; and vice versa in the frequency range near 12 Hz. In such a case, it is difficult to obtain an accurate cross-correlation estimate when the data length of the sample is rather small.

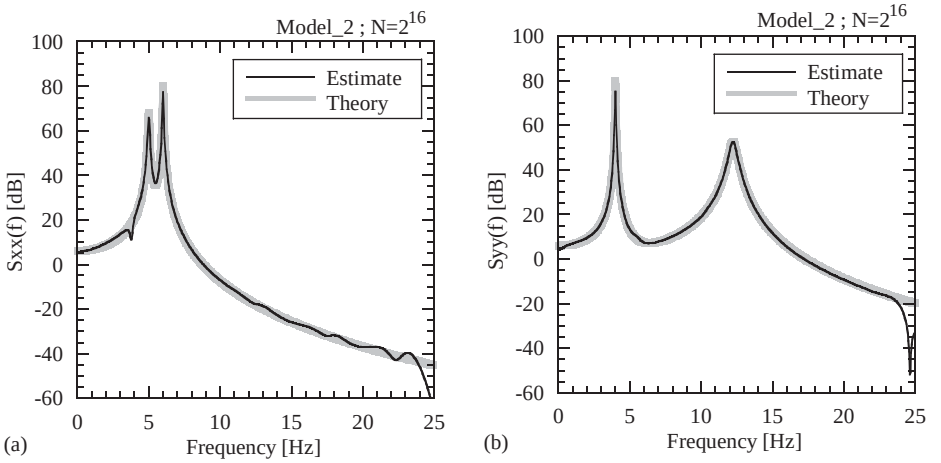

Fig. 9. Auto-PSD estimates of (a) $x(t)$ and (b) $y(t)$ in Example 2, where the number of the sample data is $N = 2^{16}$; the order of each model is $m = 10$.

Table 8
Estimated eigen properties for the frequencies f_1, f_2, the damping coefficients h_1, h_2 and the modal amplitude ratio ϕ_{p1}/ϕ_{q1}, ϕ_{p2}/ϕ_{q2} in Example 2, where the order of ARMAMA model is $m = 10$

N	1st Mode			2nd Mode		
	f_1 (Hz)	h_1 (%)	$\lvert\gamma_{xy}/\gamma_{xx}\rvert$ (·)	f_2 (Hz)	h_2 (%)	$\lvert\beta_{xy}/\beta_{yy}\rvert$ (·)
2^{10}	5.63	8.42	0.092	12.45	1.48	0.029
2^{12}	4.88	2.16	0.070	12.40	2.88	0.032
2^{14}	4.94	3.40	0.041	12.34	2.88	0.032
2^{16}	5.01	1.19	0.046	12.25	2.36	0.020
2^{18}	5.01	1.17	0.044	12.26	2.45	0.020
2^{20}	5.00	0.94	0.048	12.25	2.48	0.019
True	5.00	1.00	0.048	12.25	2.45	0.020

The poles of the first and second modes were obtained by $A_x(z) = 0$ and $A_y(z^{-1}) = 0$ respectively.
N denotes the number of the data length.
$|\beta_{xy}/\beta_{yy}|$ and $|\gamma_{xy}/\gamma_{xx}|$ denote the absolute values of the residue ratio of the cross-PSD to the auto-PSD.

7. Application to real-life record

To demonstrate the practicality of the present spectral procedure, vibration records of a 10-story office building against strong wind have been analyzed. Generally, in observation of wind responses, one can obtain the response at some parts of a building and wind records near the building; however, one cannot exactly measure wind forces acting on the building. In such a case, the system identification based on an input–output relationship cannot be employed any longer,

Table 9
Estimated noise properties for the frequencies f_p, f_q and the damping coefficients h_p, h_q in Example 2, where the order of ARMAMA model is $m = 10$

N	Noise ε_p		Noise ε_q	
	f_p (Hz)	h_p (%)	f_q (Hz)	h_q (%)
2^{10}	6.00	1.35	4.03	0.45
2^{12}	6.00	0.42	4.00	0.65
2^{14}	6.00	0.44	3.99	0.67
2^{16}	6.00	0.56	4.00	0.66
2^{18}	6.00	0.52	4.00	0.52
2^{20}	6.00	0.49	4.00	0.51
True	6.00	0.50	4.00	0.50

N denotes the number of the data length.

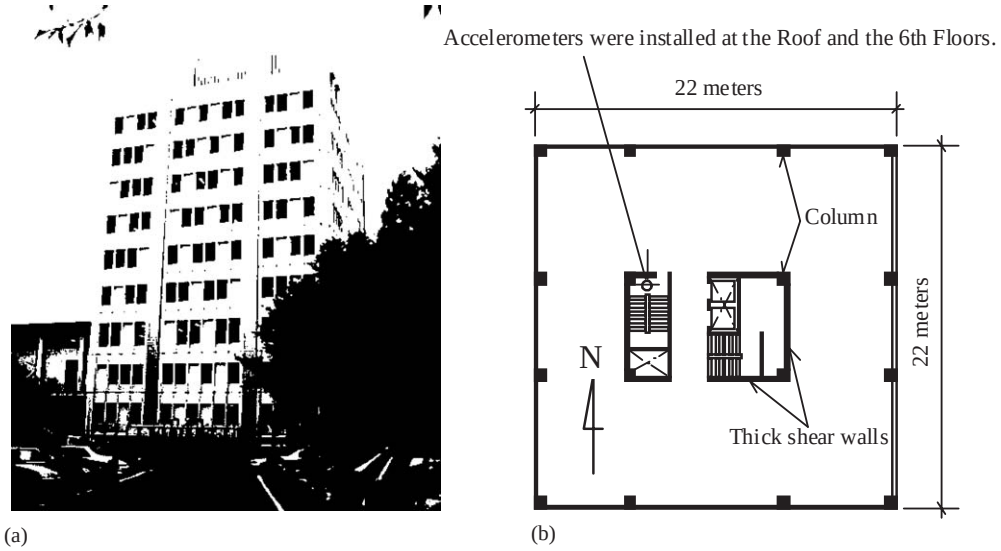

Fig. 10. A steel reinforced concrete building: (a) overviews; (b) plan and sensor location.

and the cross-spectrum-based technique should be effective to analyze the dynamic characteristics of the existing building.

Fig. 10 shows the office building, which is a steel reinforced concrete structure, and the sensor location. In this practice, two accelerometers on the east–west directions were used, which were installed at the roof and the 6th floor. The measuring was conducted when the 21st typhoon in 2002 passed through the building from October 1 to 2, 2002. The records were obtained for 24 h with the sampling period 24 Hz, and all records are divided into 144 sample segments by every 10 min to analyze the response of the building in frequency range; the number of each sample

segment equals 14,400. Hereafter, the vibration records at the roof and the 6th floor are treated as $x(t)$ and $y(t)$, respectively.

Fig. 11 shows the wind record near the building and variances of the two vibration records. Here, the wind record for every 1 h was obtained at the weather observation station of the Japan Meteorological Agency [28], which is located very close to the building, and the variances of the vibration record were calculated for every 10 min. At 9 p.m., the eye of the 21st typhoon passed above the building toward the east–northeast direction. Around this time, both the wind velocity and the amplitudes of the building response are large. This means, with the approach of the typhoon, the wind became strong and the vibration level of the building became large. Moreover, at 9 p.m., the wind direction suddenly changed and the building response became quite small for a moment. As the building was within the eye of the typhoon, the wind load acting on the building became quite small, thus the response of the building also became quite small. In Fig. 11(b), the wind velocity record at 9 p.m., does not seem to be quite small due to low time resolution (hourly averaged value).

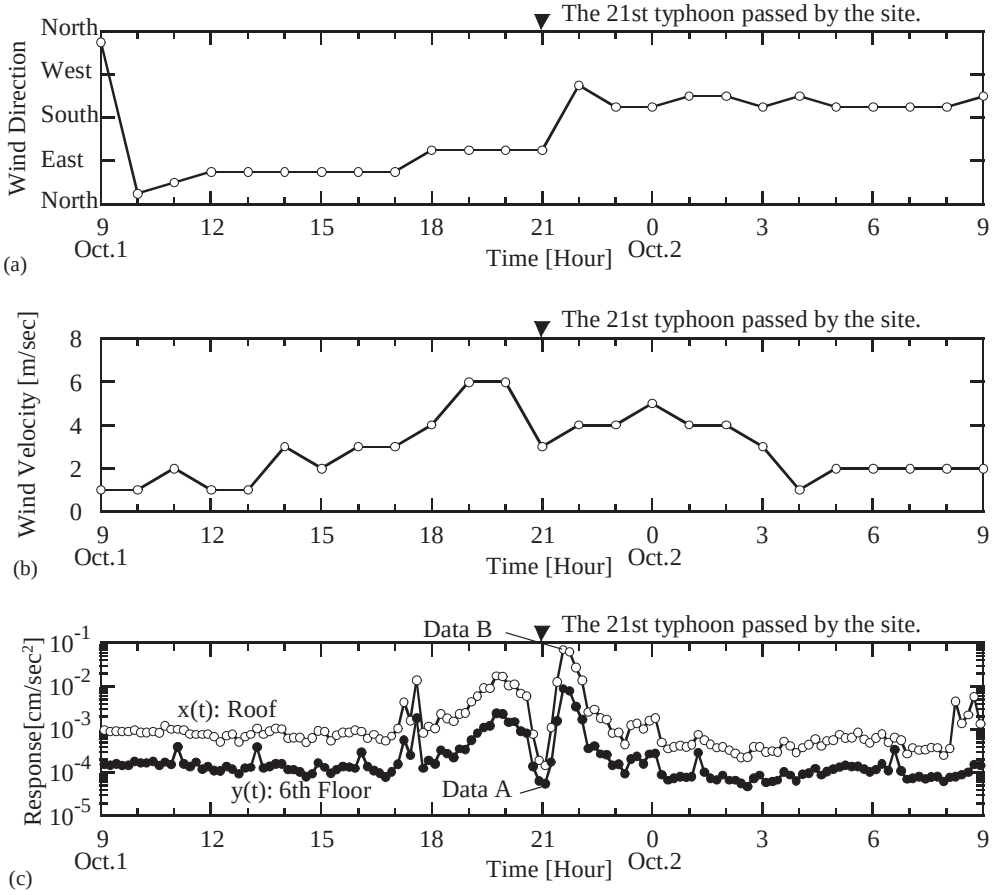

Fig. 11. Wind observation records averaged for every 1 h and variances of the building response records in every 10 min: (a) wind direction; (b) wind velocities; (c) variances of the response.

For 144 sample segments, the spectral analysis is conducted by using the present procedure and the FFT. In the use of the present procedure, the order of the ARMAMA model is set to 20, to converge the spectral form with changing the order. The other calculation condition is the same as in the previous section. On the other hand, in the use of the FFT, after the sample segments are divided into 14 small samples with no overlapping, the final PSD results are described as the average of 14 PSD estimates of the small samples; e.g., the number of the small samples is set to 2^{10}.

Fig. 12 shows examples of the cross- and auto-PSD estimated from the weak wind records and the strong wind records, where the weak and strong wind records are corresponding to the Data A and Data B shown in Fig. 11, respectively. In both wind conditions, the present procedure gives the average results of the cross- and auto-PSD by the FFT. Especially, the two resonance peaks of

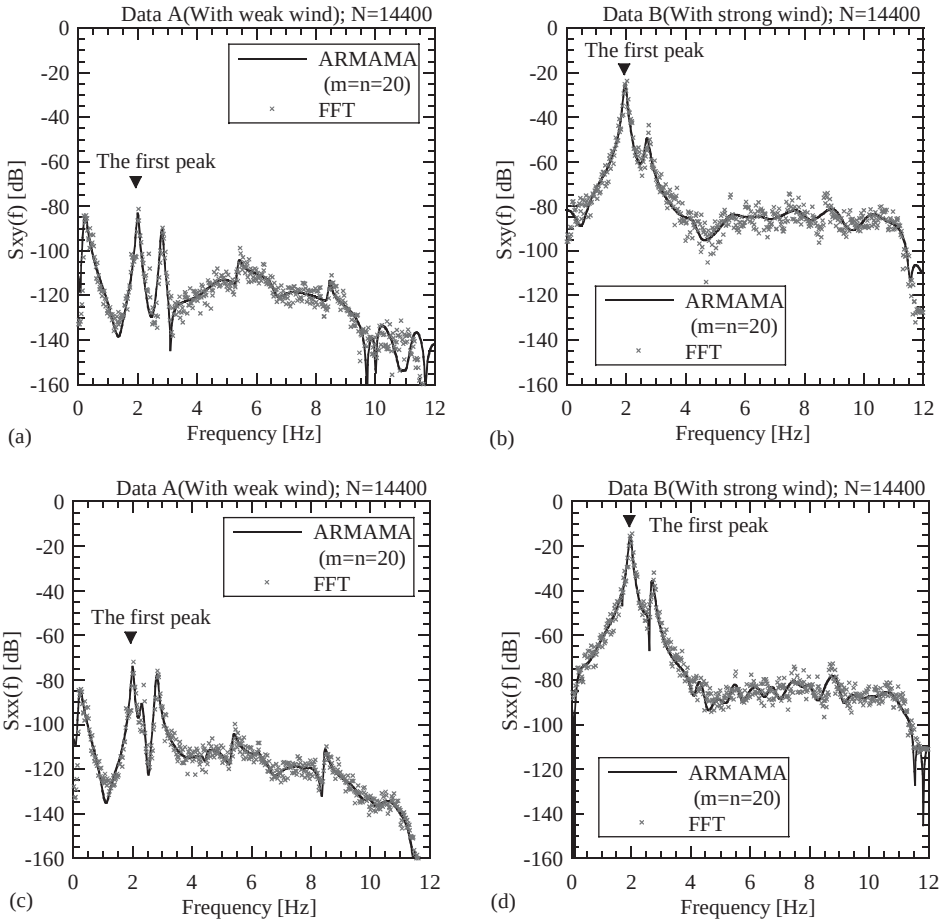

Fig. 12. Spectrum forms of the experimental records estimated by the proposed method and FFT, where the number of sample data $N = 14,400$; (a) cross-PSD of records for weak wind; (b) cross-PSD of records for strong wind; (c) auto-PSD of records for weak wind; (d) auto-PSD of records for strong wind, where the records for weak and strong winds are the Data A and Data B shown in Fig. 11(c), respectively.

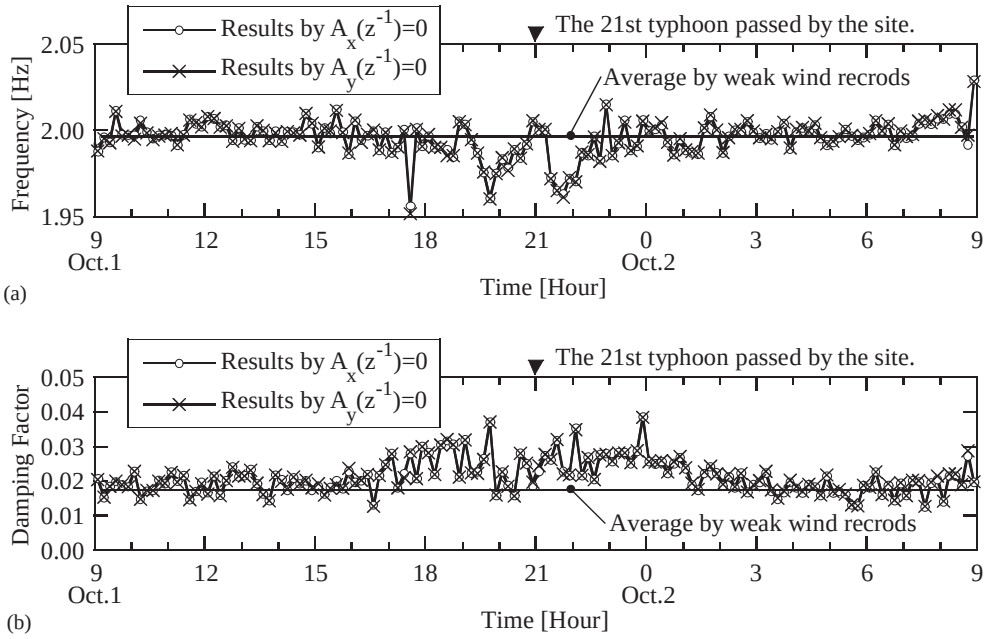

Fig. 13. The first eigenproperties of the building estimated by the proposed method for every 10 min records, which are shown as the first peak in Fig. 12: (a) nature frequency; (b) damping factor.

2.0 and 2.8 Hz can be extracted sharply whether or not the wind affects the response of the building, which correspond to the dynamic characteristics of the building.

Of two resonance peaks, the first peak of 2.0 Hz will be investigated in detail. Fig. 13 shows time fluctuations of the natural frequency and the damping factor, which are calculated from the first peak of cross-PSDs by using the relation of poles and eigenvalues in Eqs. (65) and (66). As shown in Figs. 11 and 13, the vibrational amplitude dependency of the eigenvalues have been observed: e.g. with increasing wind velocity and the response of the building, the natural frequency tends to decrease, whereas the damping factor tends to increase. In this way, the physical parameters are directly estimated from the identified forms of cross-PSDs.

8. Conclusion

The spectral analysis procedure of the cross- and auto-PSDs is presented using a pair of ARMAMA models as two observable outputs. In the procedure, firstly the cross-PSD is estimated from the observed cross-correlation function of the two outputs. Then the auto-PSD can be obtained from the observed auto-correlation and the parameter estimates of the cross-PSD. By using the proposed procedure, the cross- and auto-PSD estimates are given as the forms of the rational polynomial equations. Thus, not only are the spectral shapes of the PSDs obtained, but also the physical parameters can easily be translated from the parameters of the PSD estimates.

In the application of the proposed procedure, the cross-correlation function plays an important role in the cross-PSD estimates. Therefore, the cross-correlation function should be as accurate as possible; that is, it should be estimated from the observed outputs whose data lengths are large enough. Once the cross-PSD is estimated, the associated auto-PSD can also be obtained accurately, because the auto-correlation functions can generally be estimated more accurately than those of cross-correlation functions.

In this paper, the schemes are shown for two observed records; however, it can be easily extended to the schemes for multivariate records, because in such multivariate cases the proposed procedure can be applied to combine a pair of every two records repetitively. Additionally, though the paper only shows a general type of ARMAMA model, it can be effective to rewrite the model into a simple form for some engineering problems. For example, for system identification of a coupled system such as Example 1 in Section 5.1, the two ARMAMA models in Eqs. (3) and (5) can be assumed to have the same AR terms of the denominator in the first terms, that is, the assumption of $A_x(z^{-1}) = A_y(z^{-1})$ can be introduced. The proposed parametric estimation of the cross- and auto-PSD will be widely employed in many kinds of engineering problems.

Appendix A. Correlation functions

The instrumental variables $u(t)$ and $v(t)$ defined in Eqs. (23) and (24) can be expressed by using the impulse responses as follows:

$$u(t) = \sum_{j=0}^{\infty} h_{dx}(j) e_x(t-j), \tag{A.1}$$

$$v(t) = \sum_{j=0}^{\infty} h_{dy}(j) e_y(t-j). \tag{A.2}$$

The cross correlation $R_{xv}(\tau)$ between $x(t)$ and $v(t)$ is given using Eqs. (16) and (A.2):

$$\begin{aligned} R_{xv}(\tau) &= E[x(t)\, v(t+\tau)] \\ &= \sum_{j=0}^{\infty} \sum_{k=0}^{\infty} h_{bx}(j) h_{dy}(k) E[e(t-j) e_y(t+\tau-k)] \\ &\quad + \sum_{j=0}^{\infty} \sum_{k=0}^{\infty} h_{dx}(j) h_{dy}(k) E[e_x(t-j) e_y(t+\tau-k)] \\ &= 0. \end{aligned} \tag{A.3}$$

The cross correlation $R_{yu}(\tau)$ between $y(t)$ and $u(t)$ is given by Eqs. (17) and (A.1):

$$R_{yu}(\tau) = E[y(t)\, u(t+\tau)]$$

$$= \sum_{j=0}^{\infty}\sum_{k=0}^{\infty} h_{by}(j)h_{dx}(k)E[e(t-j)e_x(t+\tau-k)] + \sum_{j=0}^{\infty}\sum_{k=0}^{\infty} h_{dy}(j)h_{dx}(k)E[e_y(t-j)e_x(t+\tau-k)] = 0. \quad (A.4)$$

The cross correlation $R_{uv}(\tau)$ between $u(t)$ and $v(t)$ is given by Eqs. (A.1) and (A.2):

$$R_{uv}(\tau) = E[u(t)\,v(t+\tau)] = \sum_{j=0}^{\infty}\sum_{k=0}^{\infty} h_{dx}(j)h_{dy}(k)E[e_x(t-j)e_y(t+\tau-k)] = 0. \quad (A.5)$$

The cross correlation $R_{xe}(\tau)$ between $x(t)$ and $e(t)$ is given by Eq. (16):

$$R_{xe}(\tau) = E[x(t)\,e(t+\tau)] = \sum_{j=0}^{\infty} h_{bx}(j)E[e(t-j)e(t+\tau)] + \sum_{j=0}^{\infty} h_{dx}(j)E[e_x(t-j)e(t+\tau)] = h_{bx}(-\tau). \quad (A.6)$$

The cross correlation $R_{ye}(\tau)$ between $y(t)$ and $e(t)$ is given by Eq. (17):

$$R_{ye}(\tau) = E[y(t)\,e(t+\tau)] = \sum_{j=0}^{\infty} h_{by}(j)E[e(t-j)e(t+\tau)] + \sum_{j=0}^{\infty} h_{dy}(j)E[e_y(t-j)e(t+\tau)] = h_{by}(-\tau). \quad (A.7)$$

The cross correlation $R_{xe_x}(\tau)$ between $x(t)$ and $e_x(t)$ is given by Eq. (16):

$$R_{xe_x}(\tau) = E[x(t)\,e_x(t+\tau)] = \sum_{j=0}^{\infty} h_{bx}(j)E[e(t-j)e_x(t+\tau)] + \sum_{j=0}^{\infty} h_{dx}(j)E[e_x(t-j)e_x(t+\tau)] = h_{dx}(-\tau). \quad (A.8)$$

References

[1] H. Akaike, Some problems in the application of the cross-spectral method, in: *Proceedings of an Advanced Seminar Conducted by the Mathematical Research Center*, 1996, pp. 81–107.
[2] H.A. Panofsky, Meteorological applications of cross-spectrum analysis, in: *Proceedings of an Advanced Seminar Conducted by the Mathematical Research Center*, 1966, pp. 109–132.
[3] C.H. Knapp, G.C. Carter, The generalized correlation method for estimation of time delay, *IEEE Transactions on Acoustics, Speech and Signal Processing* ASSP-24 (4) (1976) 320–327.
[4] H. Pozidis, A.P. Petropulu, Cross-spectrum based blind channel identification, *IEEE Transactions on Signal Processing* 45 (12) (1997) 2977–2992.
[5] M.J. Schulz, P.F. Pai, A.S. Naser, S.K. Thyagarajan, G.R. Brannon, J. Chung, Locating structural damage using frequency response reference functions and curvatures, in: *Proceedings of the International Workshop on Structural Health Monitoring*, Stanford University, 1997, pp. 690–701.
[6] J.F. Kinkel, J. Perl, L. Scharf, A. Stubberud, A note on covariance-invariant digital filter design and autoregressive-moving average spectral estimation, *IEEE Transactions on Acoustics, Speech and Signal Processing* ASSP-27 (1979) 200–202.
[7] M. Kaveh, High resolution spectral estimation for noisy signals, *IEEE Transactions on Acoustics, Speech and Signal Processing* ASSP-27 (1979) 286–287.
[8] J.A. Cadzow, High performance spectral estimation—a new ARMA method, *IEEE Transactions on Acoustics, Speech and Signal Processing* ASSP-28 (1980) 524–529.
[9] S.M. Kay, A new spectral estimator, *IEEE Transactions on Acoustics, Speech and Signal Processing* ASSP-28 (1980) 585–588.
[10] J.A. Cadzow, Spectral estimation: an overdetermined rational model equation approach, *Proceedings of the IEEE* 70 (9) (1982) 907–939.
[11] B. Friedlander, Instrumental variable methods for ARMA spectral estimation, *IEEE Transactions on Acoustics, Speech and Signal Processing* ASSP-31 (1983) 404–415.
[12] R.L. Moses, J.A. Cadzow, A.A. Beex, A recursive procedure for ARMA modeling, *IEEE Transactions on Acoustics, Speech and Signal Processing* ASSP-33 (4) (1985) 1188–1196.
[13] S. Prasad, K.V.S. Hari, Improved ARMA spectral estimation using the canonical variate method, *IEEE Transactions on Acoustics, Speech and Signal Processing* ASSP-35 (6) (1987) 900–903.
[14] X.D. Zhang, H. Takeda, An approach to time series analysis and ARMA spectral estimation, *IEEE Transactions on Acoustics, Speech and Signal Processing* ASSP-35 (9) (1987) 1303–1313.
[15] G.E. Box, G.M. Jenkins, *Time Series Analysis, Forecasting and Control*, third ed., Holden-Day, San Francisco, 1970.
[16] L. Ljung, *System Identification: Theory for the User*, second ed., Prentice-Hall, Englewood Cliffs, NJ, 1999.
[17] E. Safak, Identification of linear structures using discrete-time filters, *Journal of Structural Engineering* 117 (10) (1991) 3064–3085.
[18] C.R. Farrar, G.H. James III, System identification from ambient vibration measurements on a bridge, *Journal of Sound and Vibration* 205 (1) (1997) 1–18.
[19] M. Covacece, A. Introini, Analysis of damage of ball bearings of aeronautical transmissions by auto-power spectrum and cross-power spectrum, *Journal of Vibration and Acoustics* 124 (2002) 180–185.
[20] M. Morf, A. Vieira, D.T.L. Lee, T. Kailath, Recursive multichannel maximum entropy spectral estimation, *IEEE Transactions on Geoscience Electronics* GE-16 (2) (1978) 85–94.
[21] T.M. Pukkila, P.R. Krishnaiah, On the use of autoregressive order determination criteria in multivariate white noise tests, *IEEE Transactions on Acoustics, Speech and Signal Processing* 36 (9) (1988) 1396–1403.
[22] S.M. Kay, *Modern Spectral Estimation*: *Theory and Application*, Prentice-Hall, Englewood Cliffs, NJ, 1988, pp. 446–478.
[23] M. Chakraborty, S. Prasad, Multichannel ARMA modeling by least squares circular lattice filtering, *IEEE Transactions on Signal Processing* 42 (9) (1994) 2304–2318.
[24] J.S. Bendat, A.G. Piersol, *Random Data*, *Analysis and Measurement Procedures*, second ed., Wiley-Interscience, New York, 1986, pp. 120–121.

[25] P.J. Brockwell, R.A. Davis, *Introduction to Time Series and Forecasting*, second ed., Springer, New York, 2002.
[26] J.A. Cadzow, B. Baseghi, T. Hsu, Singular-value decomposition approach to time series modelling, *Proceedings of the IEEE* 130 (3) (1983) 202–210.
[27] B. Peeters, G.D. Roeck, Stochastic system identification for operational modal analysis: a review, *Journal of Dynamic Systems, Measurement, and Control* 123 (2001) 659–667.
[28] Japan Meteorological Agency, Japan Meteorological Business Support Center, AMeDAS Annual Report 2002, Preliminary Version (CD-ROM), 2003.